Climate Dynamics (2006) 26: 687–711
DOI 10.1007/s00382-006-0109-9

T. M. Lenton · M. S. Williamson · N. R. Edwards
R. Marsh · A. R. Price · A. J. Ridgwell
J. G. Shepherd · S. J. Cox · The GENIE team

Millennial timescale carbon cycle and climate change in an efficient Earth system model

Received: 11 August 2005 / Accepted: 5 December 2005 / Published online: 15 March 2006

Abstract A new Earth system model, GENIE-1, is presented which comprises a 3-D frictional geostrophic ocean, phosphate-restoring marine biogeochemistry, dynamic and thermodynamic sea-ice, land surface physics and carbon cycling, and a seasonal 2-D energy-moisture balance atmosphere. Three sets of model climate parameters are used to explore the robustness of the results and for traceability to earlier work. The model versions have climate sensitivity of 2.8–3.3°C and predict atmospheric CO_2 close to present observations. Six idealized total fossil fuel CO_2 emissions scenarios are used to explore a range of 1,100–15,000 GtC total emissions and the effect of rate of emissions. Atmospheric CO_2 approaches equilibrium in year 3000 at 420–5,660 ppmv, giving 1.5–12.5°C global warming. The ocean is a robust carbon sink of up to 6.5 GtC year^{-1}. Under 'business as usual', the land becomes a carbon source around year 2100 which peaks at up to 2.5 GtC year^{-1}. Soil carbon is lost globally, boreal vegetation generally increases, whilst under extreme forcing, dieback of some tropical and sub-tropical vegetation occurs. Average ocean surface pH drops by up to 1.15 units. A Greenland ice sheet melt threshold of 2.6°C local warming is only briefly exceeded if total emissions are limited to 1,100 GtC, whilst 15,000 GtC emissions cause complete Greenland melt by year 3000, contributing 7 m to sea level rise. Total sea-level rise, including thermal expansion, is 0.4–10 m in year 3000 and ongoing. The Atlantic meridional overturning circulation shuts down in two out of three model versions, but only under extreme emissions including exotic fossil fuel resources.

T. M. Lenton (✉) · M. S. Williamson
Tyndall Centre, UK and School of Environmental Sciences, University of East Anglia, Norwich, UK
E-mail: t.lenton@uea.ac.uk
Tel.: +44-1603-591414
Fax: +44-1603-591327

N. R. Edwards
Earth Sciences, Open University, Milton Keynes, UK

R. Marsh · J. G. Shepherd · M. S. Williamson
Tyndall Centre, UK and National Oceanography Centre, Southampton, UK

A. R. Price · S. J. Cox
Southampton e-Science Centre, University of Southampton, Southampton, UK

A. J. Ridgwell
Department of Earth and Ocean Sciences, University of British Columbia, Vancouver, Canada

The GENIE team
URL: http://www.genie.ac.uk/people

1 Introduction

The amount of fossil fuel carbon that humans choose to emit to the atmosphere will be the dominant factor determining global warming on a multi-centennial timescale (Lenton and Cannell 2002). Although there is still a factor of three or more uncertainty in climate sensitivity (the equilibrium temperature change for a doubling of atmospheric CO_2) (Houghton et al. 2001), even this is overwhelmed by the potential range in CO_2 emissions and consequent atmospheric CO_2. Thus far we humans have emitted roughly 290 GtC to the atmosphere from fossil fuel burning (Marland et al. 2003) and roughly 156 GtC from land-use change (Houghton and Hackler 2002). Although conventional oil, gas and coal reserves total between 829 and 1,501 GtC, estimates of the global recoverable fossil fuel resource including oil shales range upwards from about 4,000 GtC. If exotic resources, especially methane hydrates, are included the total may be 15,000–25,000 GtC (Hasselmann et al. 1997).

The response of the global carbon cycle and surface temperature to anthropogenic CO_2 emissions will have a characteristic millennial timescale set by the rate of ocean overturning. By the year 3000, fossil fuel carbon added to the atmosphere will have largely been apportioned between the ocean, atmosphere and land surface

and the exchange of CO_2 between these components of the Earth system will be close to equilibrium (Lenton 2000). Dissolution of carbonate sediments will exceed their replenishment by carbonate weathering thus generating a small ongoing carbon sink that will remove much of the remaining fossil CO_2 from the atmosphere over $\approx 10^4$ year. We ignore this here because its impact on atmospheric CO_2 is estimated to be small over the first millennium (Archer et al. 1998), driving an additional reduction of at most 50 ppmv (A. J. Ridgwell, personal communication).

Existing studies of millennial timescale climate change have been reviewed elsewhere (Lenton 2006). They are relatively scarce and tend to be incomplete, focussing on one or two key variables, for example, the fate of the ocean circulation (Rahmstorf and Ganopolski 1999) or the ice sheets (Huybrechts and Wolde 1999). Idealized CO_2 doubling or quadrupling experiments with a few atmosphere-ocean general circulation models (AOGCMs) have been integrated for multiple centuries (Houghton et al. 2001) but plausible CO_2 scenarios have yet to be used in multi-centennial integrations with such models. The long-term response of the carbon cycle has been assessed with simple box models, one or two of which include coupling to surface temperature (Lenton 2000), but these lack spatial dimensions, a hydrological cycle or other climate variables. Thus, a comprehensive, self-consistent assessment of potential millennial timescale carbon cycle and climate change is lacking.

To address this we have developed a new Earth system model of intermediate complexity (EMIC), in a collaboration between the Grid ENabled Integrated Earth system model (GENIE) project (http://www.genie.ac.uk) and the Tyndall Centre for Climate Change Research. We call the model 'GENIE-1'. At its core is an ocean-atmosphere-sea ice climate model described in Edwards and Marsh (2005), consisting of a 3-D frictional geostrophic ocean model, an energy moisture balance atmosphere (EMBM) and a dynamic and thermodynamic sea-ice model. To this we have added a new land surface physics and terrestrial carbon model, the Efficient Numerical Terrestrial Scheme (ENTS) (Williamson et al. 2006) and an ocean biogeochemical model, BIOGEM (Ridgwell 2001) with a well mixed atmospheric chemistry box, thus closing the carbon cycle. The addition of carbonate sediments will be described in future work.

GENIE-1 has been designed for speed, to enable paleoclimate simulations, long-term future projections, large ensemble sensitivity studies, and coupling in an integrated assessment system. Hence our choice of a single layer atmosphere model rather than a 3-D dynamical atmosphere model. Within the GENIE project an atmospheric GCM is also being used, but it is orders of magnitude slower and has yet to be coupled to the carbon cycle components. The EMBM uses prescribed wind fields, and as such no effects or feedbacks due to changing atmospheric circulation patterns can be captured. However, the EMBM has been improved from Edwards and Marsh (2005) by including seasonality, coupling to a land surface model, separating surface and atmosphere/cloud albedo, and revising the precipitation function.

GENIE-1 is one of a growing number of coupled carbon cycle-climate models. At present, these include GCMs from the Hadley Centre (Cox et al. 2000) and IPSL (Friedlingstein et al. 2001), EMICs including the UVic model (Matthews et al. 2005) and the Bern 2.5-D model (Joos et al. 1999), and simple box models (Lenton 2000). A Coupled Carbon Cycle Climate Model Intercomparison Project (C4MIP) seeks to keep track of this burgeoning field (Friedlingstein et al. 2006). GENIE-1 is distinctive in that it includes a 3-D ocean and a 2-D land surface physics and carbon cycle yet it is still computationally very efficient. We can achieve up to 5,000 years of model integration in 1 CPU hour on a single 64-bit processor. In the spectrum of model complexity (Claussen et al. 2002), GENIE-1 has greater dimensionality than the Bern 2.5-D model but less than AOGCMs. Its dimensionality is equivalent to the UVic model (Weaver et al. 2001) but it has lower resolution, reduced ocean physics, and is faster.

The focus of existing studies with coupled carbon cycle-climate general circulation models (C4GCMs) has been on the century timescale response to CO_2 emissions, partly at least because these models are extremely computationally demanding. Interestingly, the Hadley and IPSL models give contrasting results. In the Hadley Centre model (HadCM3LC), when global warming passes a critical temperature the land surface switches from being a sink for atmospheric carbon to being a net source (Cox et al. 2000). This is dominated by widespread loss of soil carbon and begins with a striking dieback of the Amazon rainforest. Carbon loss from the land surface generates a positive feedback increasing the levels of atmospheric CO_2 and therefore global warming. However, in the IPSL model the land surface remains a carbon sink to year 2100 because the CO_2 fertilization negative feedback exceeds the carbon cycle-climate positive feedbacks on this timescale. Studies with simple models suggest a switch from land carbon sink to source is to be expected (Lenton 2000; Lenton and Huntingford 2003) although the timing is sensitive to uncertainties in vegetation and soil responses.

The paper is organized as follows: In Sect. 2 we briefly describe the model and various improvements made. Section 3 covers the methodology of model spin-up, tuning, historical forcing and future emissions scenarios. Section 4 describes the pre-industrial state and response to historical forcing. Section 5 describes the long-term future response. Section 6 discusses the implications for potential millennial timescale changes in the climate and carbon cycle. Section 7 concludes.

2 Model description

Our Earth system model comprises atmosphere, ocean, sea-ice, land surface physics and carbon cycle, and marine biogeochemistry components (Fig. 1). It is based

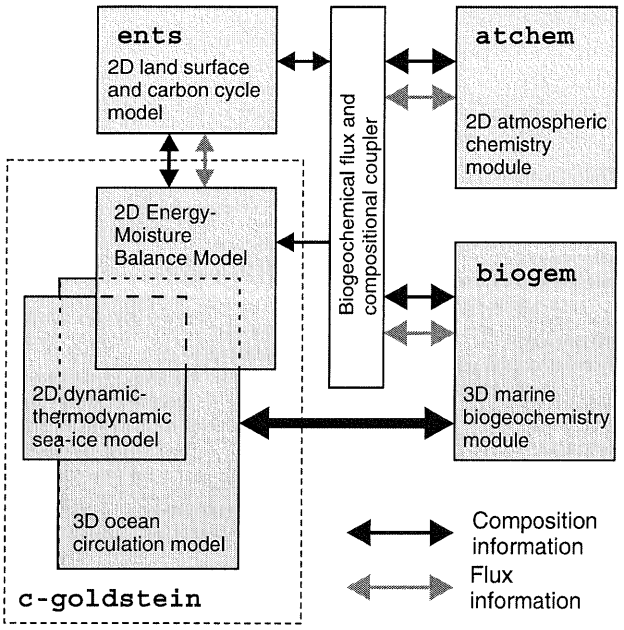

Fig. 1 Schematic of the GENIE-1 efficient Earth system model. In the version used herein, 'atchem' is simply a well-mixed reservoir of atmospheric CO_2

on the ocean-atmosphere-sea-ice model C-GOLDSTEIN (Edwards and Marsh 2005). All of the components are described in detail elsewhere. Here we give brief descriptions and concentrate on alterations made to the atmosphere model to couple to the land surface physics and carbon cycle.

2.1 Ocean and sea-ice

The frictional geostrophic ocean model, GOLDSTEIN, is three dimensional, but significantly more efficient than extant 3-D global ocean models based on the primitive equations (Edwards and Marsh 2005). The model has eight depth levels and shares a sine(latitude)-longitude horizontal grid of 36×36 equal area grid cells (≈5°×10°) with the other components of the coupled model. The sea-ice component is a dynamic and thermodynamic model based on Semtner (1976) and Hibler (1979).

2.2 Atmosphere and surface albedo

The atmospheric energy moisture balance model (EMBM) is based on that of Fanning and Weaver (1996) and Weaver et al. (2001). Here the main changes from the version used in Edwards and Marsh (2005) are the inclusion of seasonality, separation of surface and atmosphere/cloud albedo, inclusion of a relaxation time for precipitation and revision of the wind fields.

Prescribed fields of atmospheric albedo are calculated by making the approximation that there are two reflective layers that make up the planetary albedo, one at the top of the atmosphere—the atmospheric albedo—and one at the surface interface, which is suitable for our 1-layer atmosphere. Neglecting multiple reflections and absorptions this gives the planetary albedo, α_p, as

$$\alpha_p = \alpha_{atm} + \alpha_s(1 - \alpha_{atm})(1 - C_A), \quad (1)$$

where α_s is the surface albedo, taken from Eq. 4 for the ocean and, for the purposes of this derivation only, from the prescribed data sets of Matthews (1985) for the land. $C_A = 0.3$ is the absorption in the atmosphere. Planetary albedo is determined from NCEP long term monthly mean reanalysis fluxes of solar radiation at the top of the atmosphere.

$$\alpha_p = \frac{Q_{SW}^{\uparrow}}{Q_{SW}^{\downarrow}} \quad (2)$$

$Q_{SW}^{\uparrow}$ is the upward solar flux at the top of the atmosphere and $Q_{SW}^{\downarrow}$ is the downward solar flux at the top of the atmosphere. The global annual mean planetary albedo is 0.378 from the NCEP fields.

Atmospheric albedo is calculated by rearranging Eq. 1.

$$\alpha_{atm} = \frac{\alpha_p - \alpha_s(1 - C_A)}{1 - \alpha_s(1 - C_A)}. \quad (3)$$

Ocean albedo is calculated as a function of solar zenith angle, Z, using the empirical formulation of Briegleb et al. (1986). Our model does not resolve the diurnal cycle of solar zenith angle and solar insolation so we calculate the ocean albedo as the daily mean value. It is given by

$$\alpha_{ocean} = \frac{\int_0^H R(Z)\cos Z\,dh}{\int_0^H \cos Z\,dh}. \quad (4)$$

$R(Z)$ is the reflectivity of the ocean based on an empirical formula (Briegleb et al. 1986) and H is the angular half-length of the day (Peixoto and Oort 1991). The cosine of the solar zenith angle is given by

$$\cos Z = \sin\phi \sin\delta + \cos\phi \cos\delta \cos h, \quad (5)$$

where ϕ is the latitude, δ is the declination of the sun and h is the hour angle from the local meridian where $h = 0$.

This gives H as

$$H = \cos^{-1}(-\tan\phi \tan\delta). \quad (6)$$

$R(Z)$ is given by the following expression:

$$R(Z) = R_{spec}(Z) + R_{diff}, \quad (7)$$

$$R_{spec}(Z) = \frac{2.6 \times 10^{-2}}{(\cos Z)^{1.7} + 0.065} + 0.15(\cos Z - 0.1)(\cos Z - 0.5)(\cos Z - 1.0). \quad (8)$$

R_{spec} is the specular reflection and R_{diff} is the diffusive reflection modelled as a constant ($= 0.06$).

In the coupled model, land surface albedo depends on what the surface is i.e. snow, vegetation, bare soil or sand, and is a function of vegetation carbon (C_υ) and soil carbon (C_s). For a snow free surface, the terrestrial surface albedo is

$$\alpha_s = f_\upsilon \alpha_\upsilon + (1 - f_\upsilon)\alpha_{soil}, \quad (9)$$

where vegetation fraction, f_υ, is a saturating function of C_υ, the albedo of vegetation $\alpha_\upsilon = 0.1$, and the albedo of soil α_{soil} is given by

$$\alpha_{soil} = \max\left\{\alpha_{peat}, (\alpha_{peat} - \alpha_{sand})\frac{0.02C_s}{0.3} + \alpha_{sand}\right\}, \quad (10)$$

where $\alpha_{peat} = 0.11$ and $\alpha_{sand} = 0.3$. If snow is present the terrestrial surface albedo is calculated as

$$\alpha_s^{snow} = (\alpha^{snow} - \alpha_\upsilon^{snow})e^{-0.461C_\upsilon} + \alpha_\upsilon^{snow}, \quad (11)$$

where $\alpha_\upsilon^{snow} = 0.3$ is the snow covered vegetation albedo and $\alpha^{snow} = 0.8$ is the albedo of a snow covered flat surface. The albedo values are from Essery et al. (2001).

The modified parameterization of precipitation, P, is given by

$$P = \frac{\rho_a h_a}{\rho_0 \tau_{pptn}}(q_a - r_{max} q_s(T_a)) \quad (12)$$

which differs from the previous formulation in substituting a timescale of relaxation, τ_{pptn}, where $\tau_{pptn} \geq \delta_t$, in place of δ_t, the model timestep. $\rho_a = 1.25$ kg m^{-3} is a reference density of air, $\rho_0 = 1{,}000$ kg m^{-3} is a reference density of water, h_a is a reference height of the atmospheric boundary layer for moisture, q_a is the atmospheric specific humidity, r_{max} is the relative humidity threshold and q_s (T_a) is the saturation specific humidity at air temperature T_a.

The prescribed annual mean wind field used for advection of moisture is replaced with a prescribed set of monthly mean fields to promote seasonal variability in the precipitation, which is important for the accurate simulation of vegetation carbon in particular regions. Vertically integrated NCEP wind fields are weighted according to moisture content, consistent with the approach used in the UVic model (Weaver et al. 2001). Interpolation between prescribed monthly forcing fields uses the method of Killworth (1996). The main limitations of our approach are that atmospheric circulation is fixed, it doesn't capture extremes in rainfall, and it has difficulty advecting enough moisture into continental interiors.

2.3 Land surface physics and carbon cycle

The Efficient Numerical Terrestrial Scheme (ENTS) (Williamson et al. 2006) has been designed as a minimal representation of land surface physics, hydrology and carbon cycling for use in a spatially resolved context. It has single pools of vegetation carbon, soil carbon and soil water at each land grid point.

CO_2 is exchanged with a well-mixed atmosphere box (the 'atchem' module in Fig. 1). Vegetation takes up CO_2 from the atmosphere through photosynthesis, and returns some of it through respiration. A flux representing leaf litter and plant mortality transfers carbon from vegetation to the soil. Soil respiration returns CO_2 to the atmosphere. Photosynthesis depends on atmospheric CO_2 following Michaelis-Menten kinetics (a hyperbolic response) with a half saturation constant of 145 ppmv taken from Lenton (2000). This gives a similar strength of CO_2 fertilization effect to the Hadley Centre TRIFFID model (Adams et al. 2004). Photosynthesis, vegetation respiration and soil respiration all have different temperature responses chosen such that ENTS accurately captures the spatial patterns of carbon storage in vegetation and soil when driven off-line with NCEP data (Williamson et al. 2006). An important feature, based on field studies, is that soil respiration is more sensitive to warming in cold boreal ecosystems than in warm tropical ones (Lloyd and Taylor 1994; Kirschbaum 1995). The capacity of the water 'bucket' in each land grid cell depends linearly on soil carbon content between limits for desert and forest. This introduces a positive feedback whereby a well vegetated region can hold more moisture in its soil.

2.4 Marine biogeochemistry

The marine biogeochemical model, BIOGEM, is based on Ridgwell (2001) and described further in Cameron et al. (2005). The scheme used here is similar to many other marine carbon cycle models (Plattner et al. 2001; Sarmiento et al. 1998). BIOGEM vertically re-distributes a set of geochemical tracers that are being advected within the ocean, according to processes of biological uptake, particulate matter remineralization and air-sea gas exchange. Here these tracers are carbon (DIC), alkalinity (ALK) and phosphate (PO_4) (in addition to temperature and salinity). Nutrients, together with DIC, are taken out of solution in the sunlit surface ocean layer through biological action and exported in particulate form (as particulate organic matter, POM) to deeper layers. As it settles through the water column, POM is subject to remineralization processes (primarily bacterial metabolism), resulting in the release of dissolved constituent species. Remineralization in the ocean is implemented according to a predetermined profile of relative sinking flux. Associated with the biological fixation of carbon is the formation of $CaCO_3$ and further removal of DIC in addition to ALK. $CaCO_3$ is similarly dissolved in the water column following a prescribed remineralization profile. All particulate material (POM and $CaCO_3$) reaching the sediment surface is instantaneously remineralized and the dissolved constituents returned to the overlying ocean cell. CO_2 is exchanged with a well-mixed atmosphere box ('atchem' in Fig. 1) across the air–sea interface.

The setup of BIOGEM is as described in Cameron et al. (2005). Surface ocean phosphate is restored toward zero with a timescale of 6 years and this drives the biological carbon pump. Restoration to zero is more self-consistent than restoring to observations, because in our future scenarios ocean circulation can change radically. This parameterization is still rather crude compared to more numerically expensive schemes with multiple nutrients and/or multiple functional types of organism.

2.5 Sea level change

Simple parameterizations of the change in sea level due to the thermal expansion of the ocean and from the melting of the Greenland ice sheet are included. The parameterization of Greenland ice sheet melt is based on the results of the millennial global warming studies of Huybrechts and Wolde (1999) in which the contribution of Greenland melt to sea level rise is approximately linear in time and temperature, above a warming threshold. Our parameterization, diagnosed from the results of Huybrechts and Wolde (1999), is a sea level rise of 0.98 mm $year^{-1}$ $°C^{-1}$ above a threshold of 2.6°C local warming from the pre-industrial annual average air temperature over Greenland. An upper bound is imposed of 7 m of sea level rise corresponding to the complete melting of the Greenland ice sheet. The Greenland meltwater is added as a freshwater flux to the surface ocean, evenly distributed among the six ocean grid boxes around Greenland.

We choose not to include changes in mass of the Antarctic ice sheets on the grounds that current projections, especially for the West Antarctic Ice Sheet, are highly sensitive to the basal flow and viscosity parameterizations (Huybrechts and Wolde 1999). The contribution of Antarctica to global sea level on the millennial timescale is of uncertain sign but is estimated to be of much smaller magnitude than Greenland melt, ranging from −0.6 m to +0.8 m (Huybrechts and Wolde 1999).

3 Methods

The coupled model is initialized with constant fields of all physical variables (including a 20°C ocean), seed fractions of vegetation over the entire land surface, and uniform ocean biogeochemical tracers. The ocean, atmosphere, sea-ice, land and ocean biogeochemistry are spun-up for 5,000 years while holding CO_2 constant at the pre-industrial concentration of 278 ppmv. This allows the slowest components of the model such as the ocean circulation and carbon cycle to reach equilibrium.

Rather than present a single set-up of the model parameters we examine the robustness of our results and their traceability to previous work by considering three different sets of model climate parameters. These represent a subjective tuning, a parameter set traceable to previous work, and an objective tuning.

The parameters chosen for tuning are listed in Table 1 and described briefly here (see Edwards and Marsh (2005) for more details). Mixing and transport in the ocean are controlled by the isopycnal (κ_h) and diapycnal (κ_v) diffusivity, a momentum drag (Rayleigh friction) coefficient (λ), and a scaling factor (W) which multiplies the observed wind stresses in order to obtain more realistic wind-driven gyres. Atmospheric heat diffusion is a peaked function of latitude with a maximum in the tropics, zero at the South pole and a non-zero minimum at the North pole, its shape specified by amplitude (k_T), width (l_d) and slope (s_d) parameters. Moisture diffusivity (κ_q) is uniform throughout. Scaling factors for the zonal advection of heat (β_T) and for the zonal and meridional advection of moisture (β_q) compensate for limited transports in the single layer atmosphere. Net freshwater transport from the Atlantic to the Pacific remains weak hence an imposed redistribution flux of freshwater (F_a) is necessary to enhance deep sinking in the North Atlantic. Laplacian diffusion of sea-ice has a constant coefficient (κ_{hi}). We add to the existing set of tunable parameters (Edwards and Marsh 2005), the relative humidity threshold (r_{max}) and timescale (τ_{pptn}) for precipitation introduced in Eq. 12.

3.1 Subjectively tuned climate parameters

First we followed the usual procedure of adjusting parameters by a sequence of single-parameter sensitivity studies to improve qualitative agreement with chosen data. Starting from a set of C-GOLDSTEIN parameters defined by a similar procedure, we focused on obtaining a reasonable representation of the spatial distribution of vegetation and soil carbon, which in turn demands a reasonable pattern of land surface precipitation. The resulting parameter set is described as 'subjective' in Table 1.

3.2 Traceable climate parameters

Subjective tuning may be sufficient for qualitative exploration of model behaviour, but suffers from the restriction that only a tiny fraction of multi-dimensional parameter space is considered when parameters are varied individually. Given the efficiency of the model, we can make use of more advanced calibration techniques, which consider the whole of the parameter space. The Ensemble Kalman Filter (EnKF) is one such approach, which produces an ensemble of instances of the model that represents a sample of the posterior probability distribution defined by prior beliefs and climate observations.

Previous studies (Annan et al. 2005; Hargreaves et al. 2004) have tuned C-GOLDSTEIN (the ocean–atmosphere-sea-ice component of the model studied here) using an EnKF and data for ocean temperature and salinity and atmospheric surface temperature and

Table 1 Climate parameter values for the different model versions: 'subjective' set are from manual tuning, 'traceable' set are from the mean of an Ensemble Kalman Filter method applied to C-GOLDSTEIN, 'objective' set are from Response Surface Modelling

Parameter	Notation	Value			Units
		Subjective	Traceable	Objective	
Ocean					
Isopyc. diff.	κ_h	2,000	4,126	7,630	$m^2\ s^{-1}$
Diapyc. diff.	κ_v	1×10^{-4}	1.81×10^{-5}	6.77×10^{-5}	$m^2\ s^{-1}$
Friction	λ	2.5	3.43	3.71	$days^{-1}$
Wind-scale	W	2	1.67	2.72	–
Atmosphere					
T diff. amp.	k_T	3.2×10^6	3.75×10^6	3.42×10^6	$m^2\ s^{-1}$
T diff. width	l_d	1	1.31	1.66	Radian
T diff. slope	s_d	0.1	0.07	0.07	–
q diff.	κ_q	1×10^6	1.75×10^6	2.86×10^6	$m^2\ s^{-1}$
T adv. coeff.	β_T	0	0.06	0.3	–
q adv. coeff.	β_q	0.4	0.14	0.59	–
FWF adjust.	F_a	0.32	0.28	0.32	Sv
RH threshold	r_{max}	0.85	0.85	0.68	–
P timescale	τ_{pptn}	4	3.65	4.14	days
Sea-ice					
Sea-ice diff.	κ_{hi}	2,000	6,249	5,958	$m^2\ s^{-1}$

Tuning methods are described in the text and parameters are detailed in Edwards and Marsh (2005) and Eq. 12

specific humidity. Here we follow Cameron et al. (2005) in taking the mean of the ensemble of Hargreaves et al. (2004) for each climate parameter, giving the set of values labeled 'traceable' in Table 1. The relative humidity threshold and timescale for precipitation are set such that the precipitation formula is identical to previous studies with C-GOLDSTEIN (Edwards and Marsh 2005; Annan et al. 2005; Hargreaves et al. 2004).

3.3 Optimized climate parameters

To obtain a new objective tuning of GENIE-1's physical climate parameters, a Kriging method (Jones et al. 1998) of Response Surface Modelling (RSM) was used following Price et al. (2006). The RSM process (Myers and Montgomery 1995) involves sampling the 14-D parameter space with a limited number (order 100) of simulations of GENIE-1. These points are selected using formal Design of Experiment methods, in this case drawing from a LPτ sequence (Statnikov and Matuzov 1995). Each simulation returns an objective function value and these are used to generate a meta-model of the underlying function using curve-fitting techniques (the Kriging method fits a stochastic process model to the data). The meta-model's response surface is searched using a Dynamic Hill Climbing algorithm (Yuret and Maza 1993) to locate its minimum and a new simulation is then executed at this point. If the true function value differs from the modelled surface estimate then the true point is added to the data set and the RSM procedure begins again. This iterative scheme is repeated until convergence on an objective function minimum is achieved. More sophisticated methods exist for updating the Krig data set, e.g. Jones et al. (1998), and the scheme adopted here does not guarantee that the global minimum of the underlying objective function will be found. However, a local minimum is well resolved and the method can be applied to almost any underlying function.

The objective function of the model error we minimize in the tuning process is taken from Edwards and Marsh (2005) and Beltran et al. (2005) where it is applied to C-GOLDSTEIN. The function is a weighted root mean square error of the ocean and atmospheric prognostic model variables compared to interpolated observational data. The prognostic variables were ocean and atmospheric temperature, ocean salinity and specific humidity, but here we use relative humidity rather than specific humidity, because specific humidity is dependent on temperature. Thus the absolute value of the function we use is not directly comparable to the previous studies with C-GOLDSTEIN. The resulting set of tuned model parameters, labeled 'objective', are given in Table 1.

A measure of the quality of the modelled surface used to find these parameters is obtained by performing a separate random sampling of the underlying function. These extra points are evaluated on the modelled surface and the correlation between the two provides a measure of the accuracy of the Krig (Keane 2003). The data for 285 independent samples of the objective function are plotted in Fig. 2. The correlation coefficient for this data is 0.9111 indicating reasonable agreement between the modelled surface and the true objective function. It is noticeable that function evaluations which have low error are predicted with more accuracy by the Krig than those with high error (points closer to the origin lie nearer to the line). This suggests that the surface is better resolved in regions closer to the optimum.

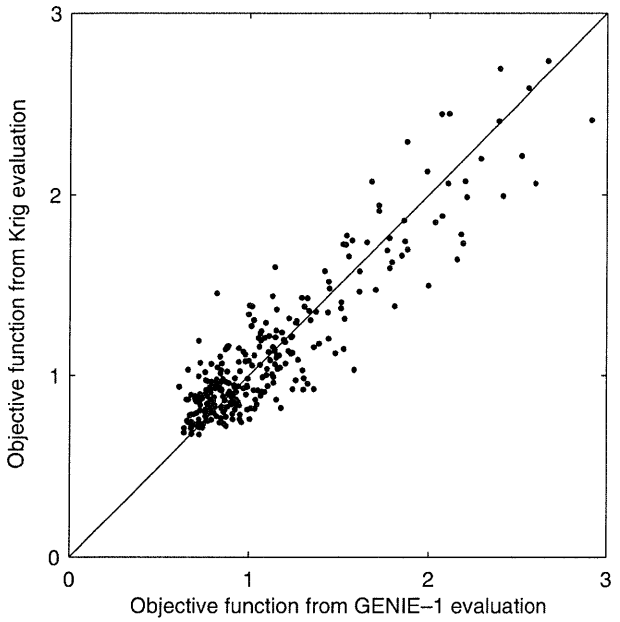

Fig. 2 Correlation between 285 random GENIE-1 objective function evaluations and those predicted by the Kriging trained on a separate set of 100 evaluations from a LPτ sequence plus 31 updates

3.4 Historical forcing

The spun-up pre-industrial state of the Earth system is used as the starting point for experiments where GENIE-1 is forced with anthropogenic CO_2 emissions up to 1990. This is taken as 'present day' because future emissions scenarios typically start in 1990. Linear fits to estimates of fossil fuel (Marland et al. 2003) and land-use change (Houghton and Hackler 2002) emissions are combined to give total CO_2 emissions, as in Lenton (2000). When comparing model output to climate data for the 1990s it is assumed (as in four of the six future scenarios) that fossil fuel emissions increased from 6 GtC $year^{-1}$ in 1990 to 7 GtC $year^{-1}$ in 2000 as in IS92a 'business as usual', and land-use change was a constant 1.4 GtC $year^{-1}$ as in Lenton (2000). There is no representation of land-use change in the model, in other words, land-use change carbon is not removed from vegetation and soil. There is no aerosol forcing, either anthropogenic or volcanic, no forcing by non-CO_2 greenhouse gases, and historical variations in solar intensity are ignored.

3.5 Long-term emissions scenarios

Six long-term future CO_2 emissions scenarios (Table 2; Fig. 9a) were chosen with the aims of: (a) spanning the range of plausible total fossil fuel emissions, (b) exploring the effects of different emissions pathways after the year 2100, (c) exploring the effects of burning the same amount of fossil fuel at different rates, and (d) traceability to previous studies. The same scenarios have been used to force a simple model by Lenton (2006).

Four of our scenarios are taken directly from Lenton (2000). The minimum scenario A is based on IS92c followed by a decline to zero emissions in 2200. The baseline scenario B allows comparison to results presented in Houghton et al. (1995). A conservative estimate of known conventional fossil fuel resources is 4,000 GtC and this forms the basis for scenarios C, emitting this reserve rapidly, and D, emitting it slowly. Hasselmann et al. (1997) have considered scenarios emitting unconventional resources including methane hydrates, which may exceed 10,000 GtC. Our upper limit scenario F, is based on the same total emissions, 15,000 GtC, as Hasselmann et al. (2003). Scenario E is intended to explore the response space between this and the 4,000 GtC scenarios C and D.

4 Model performance up to present

The three model variants (climate parameter sets) are referred to from here on as 'subjective' (subjectively tuned), 'traceable' (from the mean of an Ensemble Kalman Filter method applied to C-GOLDSTEIN), and 'objective' (from RSM). Their root mean square (rms) errors compared to ocean temperature, salinity, surface air temperature and specific humidity data are 0.625 (subjective), 0.566 (traceable), 0.634 (objective). The objective tuning is poor here because it used relative humidity rather than specific humidity as a tuning target. Substituting relative humidity for specific humidity data the rms errors are 0.730 (subjective), 0.617 (traceable), 0.618 (objective). The fact that the objective tuning fails to improve on the traceable parameter set, despite using relative humidity as a tuning target, suggests it is only finding a local minimum in model parameter space.

4.1 Pre-industrial state

The pre-industrial global annual mean air temperatures at sea level are 11.92°C (subjective), 11.46°C (traceable), 10.13°C (objective), all rather cold compared to estimates of ≈14°C (from NCEP data for present minus observed warming). The corresponding planetary albedos are 0.375, 0.371, 0.369, all slightly below the 0.378 diagnosed from observations. Note that the tuning process considered only transport parameters, thus the global mean heat balance is only indirectly affected. Furthermore the global mean was not a target for the tuning process, because spatially explicit data were used.

Equilibrium vegetation and soil carbon storage are shown in Fig. 3 together with results for the ENTS model driven off-line with NCEP data (Williamson et al. 2006). All three model versions simulate total vegetation and soil carbon stores within the uncertainties in observations. Global vegetation carbon inventories are

Table 2 Long-term future CO_2 emissions scenarios used to force GENIE-1

Label	Total emissions (GtC)	1990–2100	Beyond 2100	Reference
A	1134	IS92c	Linear decline to zero in 2200	Lenton (2000) scenario 2
B	2660	IS92a	Linear decline to zero in 2200	Lenton (2000) scenario 1, from Houghton et al. (1995)
C	4000	IS92a	Linear decline to zero in 2332	Lenton (2000) scenario 4
D	4000	1990 level	Linear decline to zero in 2926	Lenton (2000) scenario 5
E	9213	IS92a	+0.16 GtC year^{-2} until 2150 then linear decline to zero in 2599	Lenton (2006)
F	15000	IS92a	+0.16 GtC year^{-2} until 2250 then linear decline to zero in 2634	Lenton (2006)

574 GtC (subjective), 542 GtC (traceable), 491 GtC (objective). Global soil carbon inventories are 1,367, 1,438, 1,416 GtC, respectively. Carbon storage increases in all versions relative to the estimates of 451 GtC in vegetation (Olson et al. 1985) and 1,306 GtC in soil (Batjes 1995) used to tune the model off-line, and the resulting off-line calculated values of 437 GtC in vegetation and 1,317 GtC in soil. The traceable parameter set is closest to IPCC values of 550 GtC in vegetation and 1,500 GtC in soil (Houghton et al. 1990) but these are not necessarily the best estimates. Deserts are less distinct in the coupled model because the atmosphere is too diffusive. Boreal forest in Eurasia is generally too sparse due to lack of moisture transport into the continental interior, and too Northerly in location.

Land carbon fluxes are 147 (subjective), 127 (traceable), 110 (objective) GtC year^{-1} for net photosynthesis, 69, 56, 45 GtC year^{-1} for vegetation respiration, and 78, 72, 65 GtC year^{-1} for leaf litter and soil respiration. The considerable range in these values is due to the differing patterns of air temperature and precipitation across the land surface in the model variants.

Equilibrium ocean carbon inventories are 35,208, 35,750, 35,503 GtC, all considerably below estimates of ≈38,000 GtC (Houghton et al. 1990). This is mostly due to the model ocean volume of 1.31×10^{18} m^3 being smaller than the real ocean volume of $\approx1.37\times10^{18}$ m^3. This in turn is due to the model ocean depth being limited to 5,000 m. The ≈550 GtC range in ocean carbon storage must be due primarily to varying effectiveness of the biological and solubility pumps in the different ocean circulation states and secondarily to differing ocean temperatures.

The spun-up Meridional Overturning Circulation (MOC) of the Atlantic, Pacific and global ocean are shown in Fig. 4 and ocean heat transport in Fig. 5. Atlantic MOC varies considerably in strength between the model variants; 24 Sv (subjective), 14 Sv (traceable), 18 Sv (objective), with the traceable version closest to an estimate of 15±2 Sv (Ganachaud and Wunsch 2000). The subjectively tuned version has a circulation pattern similar to Edwards and Marsh (2005) with strong diapycnal diffusivity (κ_v) probably contributing to the strength of the Atlantic meridional overturning circulation (Toggweiler and Samuels 1998). The traceable version resembles Hargreaves et al. (2004) from which its parameters were derived, indicating that adding land surface physics and altering the atmospheric physics have not greatly affected the ocean circulation. The objectively tuned version has poor Atlantic MOC in that the maximum is shifted to the sub-tropics. Its intermediate MOC strength is consistent with its intermediate value for diapycnal diffusivity (κ_v).

4.2 Present climate

Surface atmospheric temperature anomalies for the three model variants relative to NCEP reanalysis data are shown in Fig. 6. Global annual average air temperatures in 1990 are 12.5°C (subjective), 12.1°C (traceable), 10.7°C (objective), in all cases colder than the observed 14.95°C from NCEP data. The latitudinal temperature gradient varies across the three model variants, due to variations in the parameters controlling atmospheric heat diffusion as a function of latitude. The temperature gradient is generally too weak and the equator too cold, because too much heat tends to be diffused away from the equator. The subjectively tuned parameters give the strongest temperature gradient and warmest equator, because they have the lowest amplitude (k_T) for atmospheric heat diffusion. The objectively tuned parameters give the weakest temperature gradient and coolest equator, partly because they have the greatest oceanic heat transport (Fig. 5). In the subjectively tuned, the Arctic and Antarctic are generally too cold, whereas in the objectively tuned, they are generally too warm, again due to the differences in latitudinal heat diffusion.

Global warming from 1800 to 1990 is 0.56°C (subjective), 0.65°C (traceable), 0.54°C (objective) compared to the observed warming from 1860 to 1990 of 0.6±0.2°C (Houghton et al. 2001). This agreement is somewhat fortuitous given that the model does not include radiative forcing due to non-CO_2 greenhouse gases or sulphate aerosols, which counteract one another, or a number of other radiative forcing factors. However, it is consistent with simpler models that have just CO_2 forcing and similar climate sensitivity (Lenton 2000).

Surface precipitation anomalies relative to NCEP reanalysis data are given in Fig. 7. This highlights the main weakness of the single layer energy-moisture

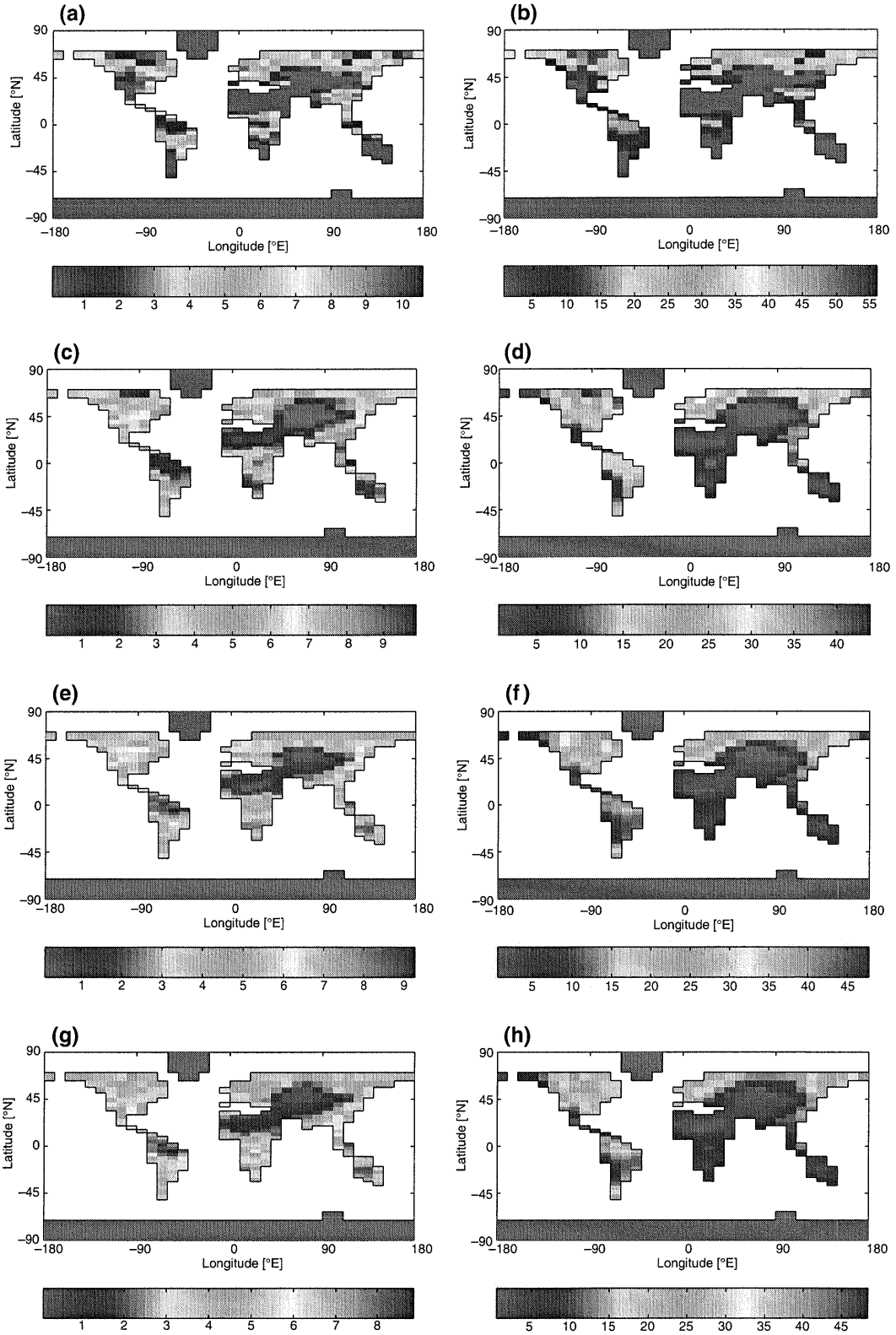

Fig. 3 Equilibrium carbon storage (kgC m^{-2}) in **a**, **c**, **e**, **g** vegetation, and **b**, **d**, **f**, **h** soil, under pre-industrial atmospheric CO_2, for **a**–**b** ENTS driven off-line with NCEP climate data (Williamson et al. 2006), and for GENIE-1 with different climate parameter sets: **c**–**d** subjective, **e**–**f** traceable, **g**–**h** objective

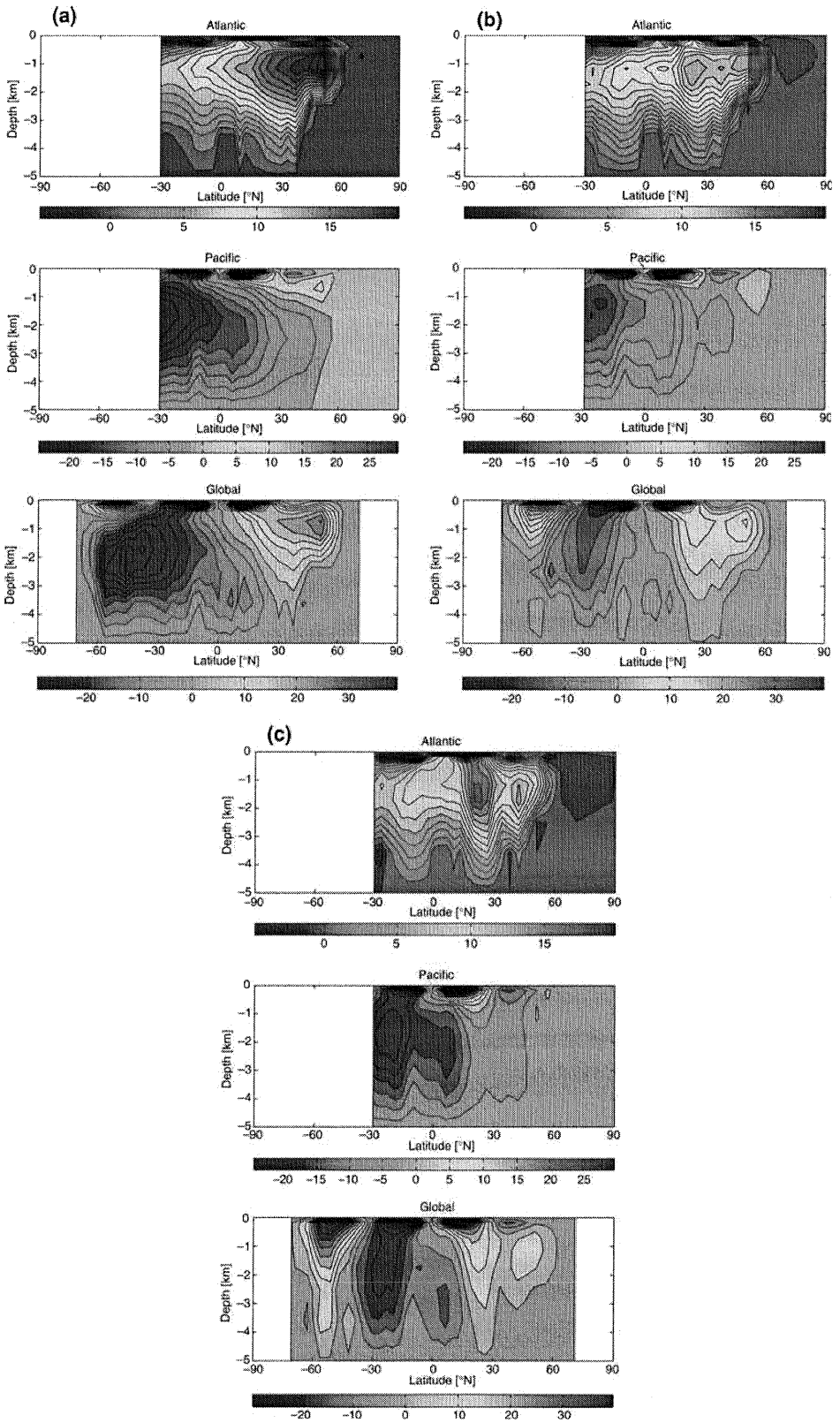

Fig. 4 Pre-industrial Atlantic, Pacific and Global Meridional Overturning Circulation (MOC), for different model climate parameter sets; **a** subjective, **b** traceable, **c** objective

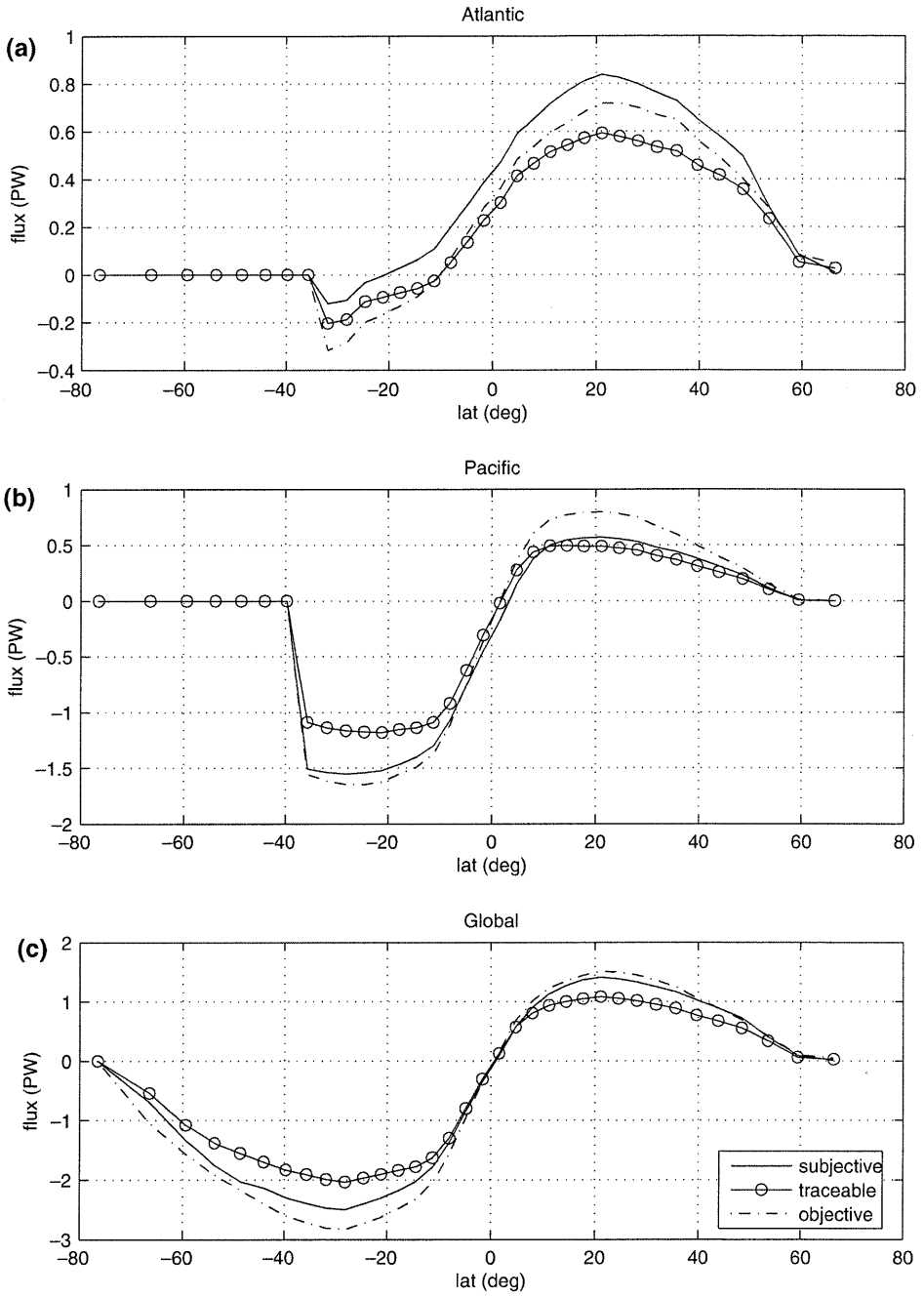

Fig. 5 Pre-industrial ocean heat transport (PW) in the different model climate parameter sets for **a** Atlantic, **b** Pacific and **c** Global

balance atmosphere model, which is too diffusive and hence has precipitation too evenly distributed. It only reaches half the observed tropical maxima in precipitation, and rains too much in the desert regions. The anomalies are smaller over large areas of temperate and boreal land surface, which is important for vegetation. There are variations in precipitation pattern between the model variants, for example in Eurasia and North America, which in turn accounts for much of the difference in initial vegetation and soil carbon. The objectively tuned model has the highest moisture diffusivity (κ_q), which gives it the most uniform rainfall. The subjectively tuned model has the lowest moisture diffusivity and consequently the greatest difficulty getting enough moisture into continental interiors, especially Eurasia. Diffusion appears to dominate over moisture advection (β_q) which is also highest in the objectively tuned model but lowest in the traceable model.

Arctic sea ice cover (not shown) is similar across the three model variants with annual average values of 9.4×10^{12} m^2 (subjective), 7.8×10^{12} m^2 (traceable), 7.4×10^{12} m^2 (objective). Actual Arctic sea ice cover ranges from 6–8×10^{12} m^2 in summer (Stroeve et al. 2005) to 14–16×10^{12} m^2 in winter (Parkinson et al. 1999). The short-

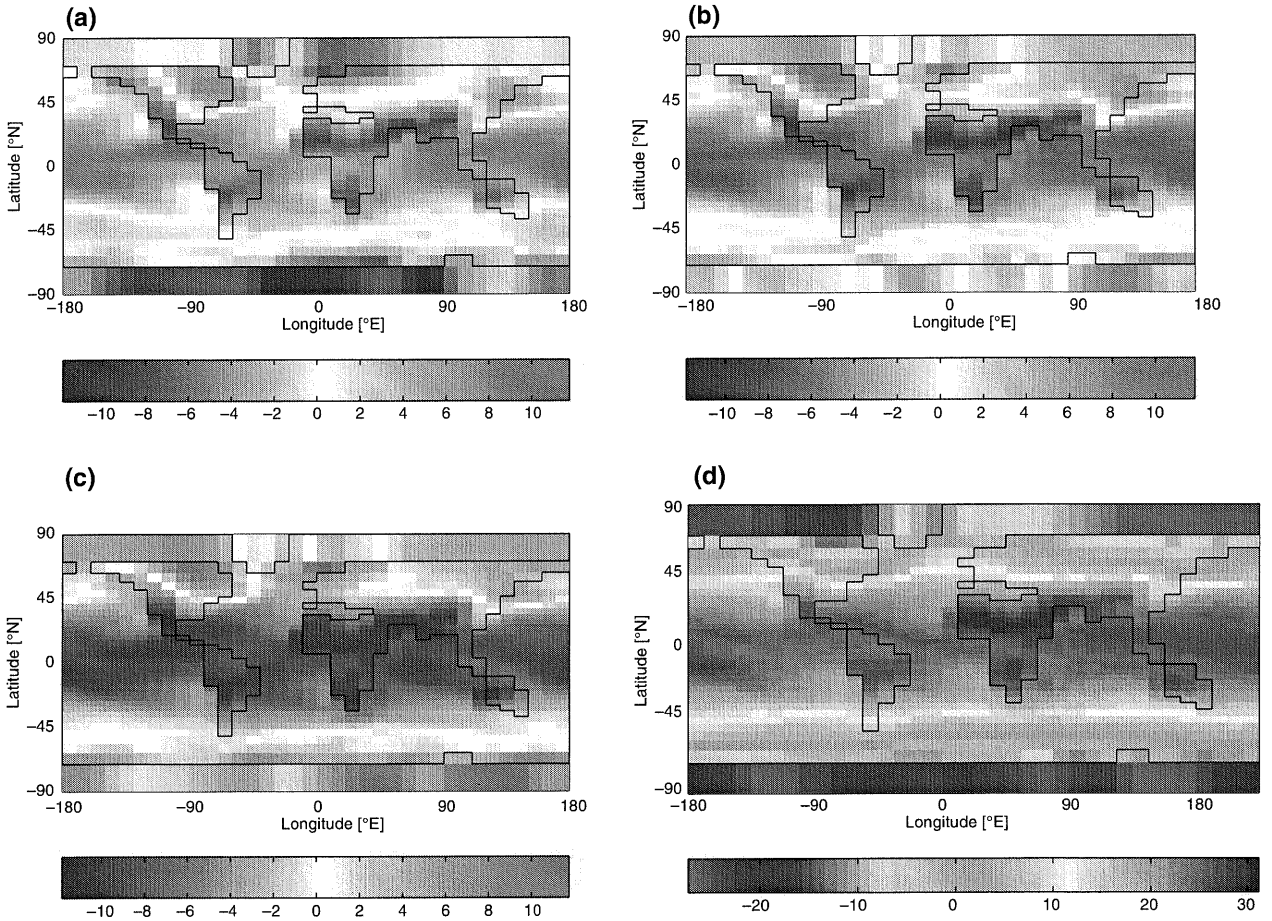

Fig. 6 Annual mean air temperature (°C) anomalies in the model in 1990 for different climate parameter sets **a** subjective, **b** traceable, **c** objective, relative to **d** NCEP data

age of Arctic sea-ice in the model is primarily due to the underestimated area of the Arctic Ocean on the model grid, but anomalous warmth in the traceable and objective versions also contributes. Antarctic sea ice cover is more variable in the model variants at 6.6×10^{12} m^2 (subjective), 5.7×10^{12} m^2 (traceable), 0.9×10^{12} m^2 (objective). Actual Antarctic sea ice cover ranges from $3\text{–}4\times10^{12}$ m^2 in summer to $17\text{–}20\times10^{12}$ m^2 in winter (Parkinson 2002). The objective parameter set gets almost no Antarctic sea ice cover because of excessive atmospheric heat diffusion, the greatest ocean heat transport to these latitudes (Fig. 5) and too much open-ocean convection, all leaving the Southern Ocean too warm. Southern Ocean temperature anomalies are less extreme and of mixed sign in the other two model variants.

Sea level change at 1990, due to thermal expansion, is 0.06 m in all model variants. This is similar to the predictions of AOGCMs (Meehl et al. 2005) and below the observed estimate of 0.15–0.2 m (Houghton et al. 2001). The discrepancy can be reconciled given recent analysis that $\approx$1.4 mm year^{-1} of the present 1.5–2.0 mm year^{-1} sea level rise is due to continental ice sheet melt (Miller and Douglas 2004).

4.3 Carbon cycle response

At the year 1990 the model variants predict atmospheric CO_2 concentrations of 345 ppmv (subjective), 354 ppmv (traceable), 345 ppmv (objective). The traceable parameter set matches observations at Mauna Loa, Hawaii (Keeling and Whorf 2005), whilst the others are 9 ppmv too low. Carbon budgets of 1980s for the three model variants are compared with that derived from observations and an estimate of land-use change emissions (Houghton et al. 2001) in Table 3. Only the traceable set has an ocean carbon sink within the estimated range, the others being too strong. The land carbon sink is probably too weak. This may be partly justified in that the model only includes CO_2 fertilization and temperature effects, whilst nitrogen fertilization and re-growth on abandoned land are thought to be contributing to the real land carbon sink. However, some other models get a larger current land carbon sink just from CO_2 fertilization and temperature effects (Lenton 2000).

The sizes of the cumulative land and ocean carbon sinks vary significantly between the model variants, as

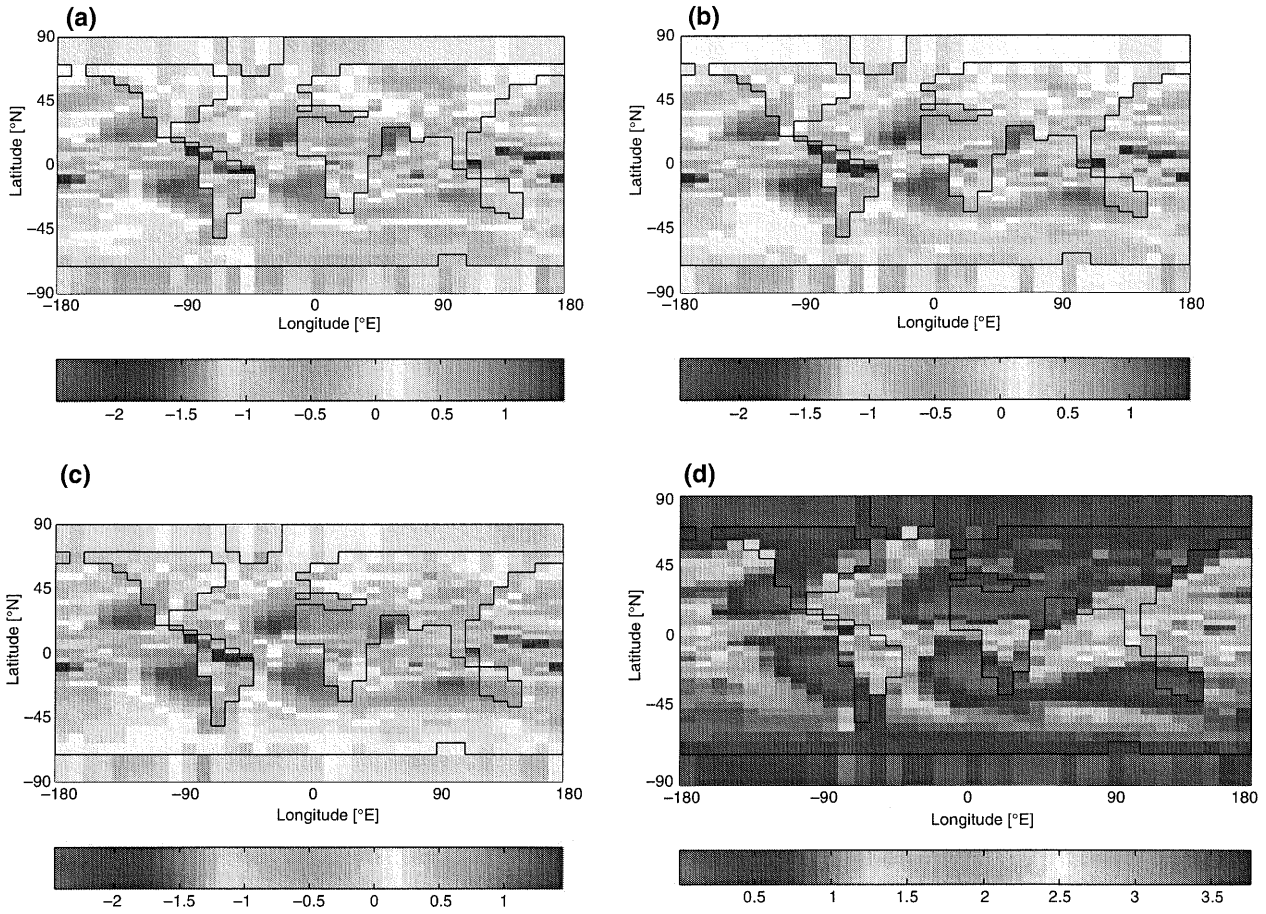

Fig. 7 Annual mean precipitation (m year^{-1}) anomalies in the model in 1990 for different climate parameter sets **a** subjective, **b** traceable, **c** objective, relative to **d** NCEP data

Table 3 The 1980s carbon budget from model variants and from House et al. (2003) updated from Houghton et al. (2001), combining observational constraints and an estimate of land-use change emissions

GtC year^{-1}	Model variant			Data estimate
	Subjective	Traceable	Objective	
Emissions (fossil + land-use)	7.0	7.0	7.0	$5.4 \pm 0.3 + 0.9$–2.8
Atmospheric increase	2.9	3.5	3.1	3.3 ± 0.1
Ocean sink	2.7	2.4	2.9	1.8 ± 0.8
Land sink	1.4	1.1	1.0	0.3–4.0

The range given for land-use change emissions represents the uncertainty in the estimates and contributes to the corresponding range in the land sink

does the apportioning of added carbon between vegetation and soil (Table 4). Integrated total emissions 1800 to 1990 are 350 GtC. An estimate of the cumulative ocean carbon sink 1800 to 1994 is 118 ± 19 GtC (Sabine et al. 2004), and the traceable parameter set is in good agreement with this with 120 GtC uptake from 1800 to 1990 and a further $\approx$10 GtC uptake in the years 1991–1994. Its cumulative land carbon sink (74 GtC) is fortuitously that required to give the observed accumulation of CO_2 in the atmosphere. In the other two

Table 4 Cumulative carbon uptake from 1800 to 1990 in the model variants

GtC	Model variant		
	Subjective	Traceable	Objective
Ocean	132	120	145
Vegetation	32	35	31
Soil	42	29	27
Total	206	184	203

model variants, the ocean sink is too strong. Excessive open ocean convection in the Southern Ocean is probably the main cause, a further contributing factor being that the 176 m depth of the top layer of the ocean model is too thick, hence too much surface water tends to equilibrate CO_2 with the atmosphere.

Annual average ocean-atmosphere CO_2 flux in 1990 is compared to observations (Takahashi et al. 2002) in Fig. 8. Regions of CO_2 uptake and release are broadly captured. Uptake in the Greenland-Iceland-Nordic seas is underestimated due to a lack of deep-water formation there in the model variants, and our coarse resolution leading to excessive sea-ice cover. Uptake in the Southern Ocean is rather extensive, due to excessive open ocean convection there, under-prediction of sea-ice cover, and perhaps also to excessive nutrient uptake without iron limitation in the model. Regions of CO_2 release and its magnitude are broadly captured, although a CO_2 source in the North Pacific is missing.

Annual average land-atmosphere CO_2 flux (not shown) represents the distribution of the land carbon sink. It does not include the net flux from land-use change, hence it cannot be directly compared with the net land-atmosphere CO_2 flux derived from inversion studies, and no equivalent data set exists. Across all model variants, the boreal forest tends to be the strongest carbon sink, and in the subjectively tuned version, the carbon sink in Amazonia is of similar magnitude, that model variant having greatest Amazonian precipitation. A boreal location for the land carbon sink plus a significant Amazonian sink are consistent with inversion studies and inferences from observations (Houghton et al. 2001).

4.4 Summary

After tuning there remain common errors in the climate of the three model variants, especially in the precipitation field and tropical temperatures. The traceable climate parameter set has the lowest rms errors with respect to present climate data, gives the best carbon

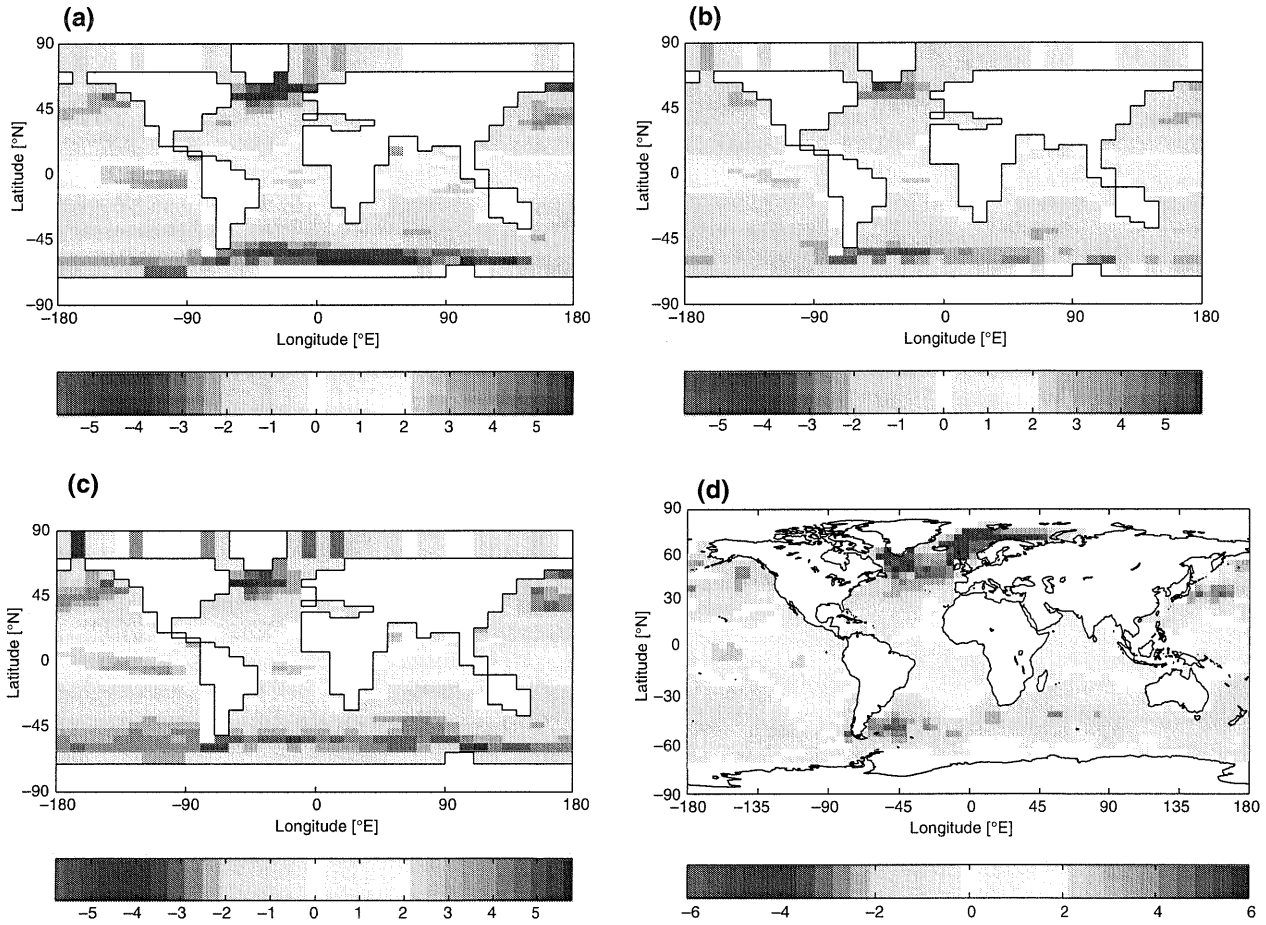

Fig. 8 Ocean-atmosphere CO_2 exchange (mol m^{-2} $year^{-1}$) in the model in 1990 for different climate parameter sets; **a** subjective, **b** traceable, **c** objective, compared to **d** observational estimates from Takahashi et al. (2002)

cycle response up to present, has an Atlantic Meridional Overturning Circulation strength close to an observational estimate, and also has reasonable pre-industrial vegetation and soil patterns of carbon storage. The subjective parameter set has a better temperature distribution, and arguably better vegetation distribution. The objectively tuned parameter set has a much improved relative humidity field, but at the cost of other aspects of the model climate. Hence we take the traceable climate parameter set as the default for future projections, and discuss the others where they deviate from it. The systematic coolness of tropical temperatures mean that upper temperature limits for vegetation will be harder to reach than in reality. However, our Greenland ice sheet melt parameterization is based on temperature change rather than absolute temperatures.

5 Long-term future response

The climate sensitivities (equilibrium temperature change for a doubling of CO_2 from pre-industrial) of the model variants are 3.3°C (subjective), 3.2°C (traceable), 2.8°C (objective). The radiative forcing due to CO_2 doubling is identical in each case, hence the differences must be due to climate feedbacks potentially involving water vapour, surface albedo and evapotranspiration. The corresponding hydrological sensitivities (increase in global precipitation under doubled CO_2) are 6.0, 5.7, and 7.4%. The climate and hydrological sensitivities put the three model variants somewhere in the middle of the suite of AOGCMs used in Houghton et al. (2001). The emission scenarios and response of key variables to year 3000 are shown for the traceable parameter set in Fig. 9 and discussed in more detail in the following sections.

5.1 Atmospheric CO_2

Atmospheric CO_2 exhibits a peaked response and is decaying toward equilibrium at the end of the millennium (Fig. 9b). Peak levels of atmospheric CO_2 range from 541 ppmv (1,100 GtC) to 5,966 ppmv (15,000 GtC). The effect of the rate of emitting 4,000 GtC is seen in the peak values of atmospheric CO_2 of 1515 ppmv in 2310 under rapid emissions (scenario C) and 1,236 ppmv in 2780 under slow emissions (scenario D). However, by the end of the millennium both have similar CO_2. For a given emissions scenario, peak atmospheric CO_2 is highest for the traceable parameter set, because the ocean carbon sink is weakest and the land becomes the largest carbon source. Peak atmospheric CO_2 varies across the model variants by a minimum of $\approx$10% in scenarios A and F and a maximum of $\approx$23% in scenario D.

The airborne fraction of added CO_2 at the end of the millennium, i.e. the fraction of added carbon still in the atmosphere, generally increases with total carbon emitted (Table 5). This is primarily due to a decline in buffering capacity of the ocean as more carbon is added (it is acidified), and secondarily due to declines in ocean and land carbon storage with global warming. The subjectively and objectively tuned model versions have lower airborne fractions (i.e. lower CO_2) than the traceable version, due primarily to stronger ocean carbon sinks.

5.2 Climate

Mean global surface air temperature peaks and then declines slightly under emissions scenarios A–C but continues increasing in scenarios D–F (Fig. 9c). For a given emissions scenario, global warming is greatest for the traceable parameter set, because it has the highest CO_2. Peak warming ranges from 2.6°C (1,100 GtC) to 12.5°C (15,000 GtC). The effect of rate of emissions is seen in the peak warming of 6.7°C in 2400, when emitting 4,000 GtC rapidly (C), as opposed to 6.3°C in 2880, when emitting 4,000 GtC slowly (D). Furthermore, the rate of warming is much slower when emitting a given amount of fossil fuel more slowly.

The threshold for Greenland ice sheet melt of 2.6°C local warming (Huybrechts and Wolde 1999) is only briefly exceeded for 1,100 GtC total emissions. In all other scenarios, Greenland melt contributes significantly to sea level rise, and it is complete in year 2900 under 15,000 GtC emissions, contributing 7 m to global sea level rise. Total global sea-level rise, including thermal expansion, ranges from 0.4 to 10 m across the scenarios and is ongoing at the end of the millennium, except in scenario A with 1,100 GtC emissions. In the other model variants, the sea level rise results are about 1 m lower for scenarios B, C, D but similar or slightly higher for scenarios E and F. Greenland finishes melting before the end of the millennium under scenario F in the subjectively tuned model but not in the objectively tuned model, because of differences in regional warming of Greenland (Fig. 10).

Annual average sea-ice cover (not shown) tends to decline, and if it disappears it does so in a rapid transition in both hemispheres. Antarctic sea-ice is lost under all but the minimum 1,100 GtC emissions scenario A. Arctic sea-ice is lost under extreme emissions scenarios E and F in the traceable and objective versions, but some remains in the subjectively tuned version. These results should be treated with caution because the initial sea-ice state is generally poor.

The spatial patterns of temperature and precipitation change in year 3000 of the 15,000 GtC scenario F are shown for the three model variants in Fig. 10. Warming is greatest in the high latitudes, in common with GCMs. The land warms faster than the ocean, but by the end of the millennium warming is almost identical over land and ocean. The lower climate sensitivity of the objectively tuned model is apparent, and there is significant variation in the pattern of warming between the model

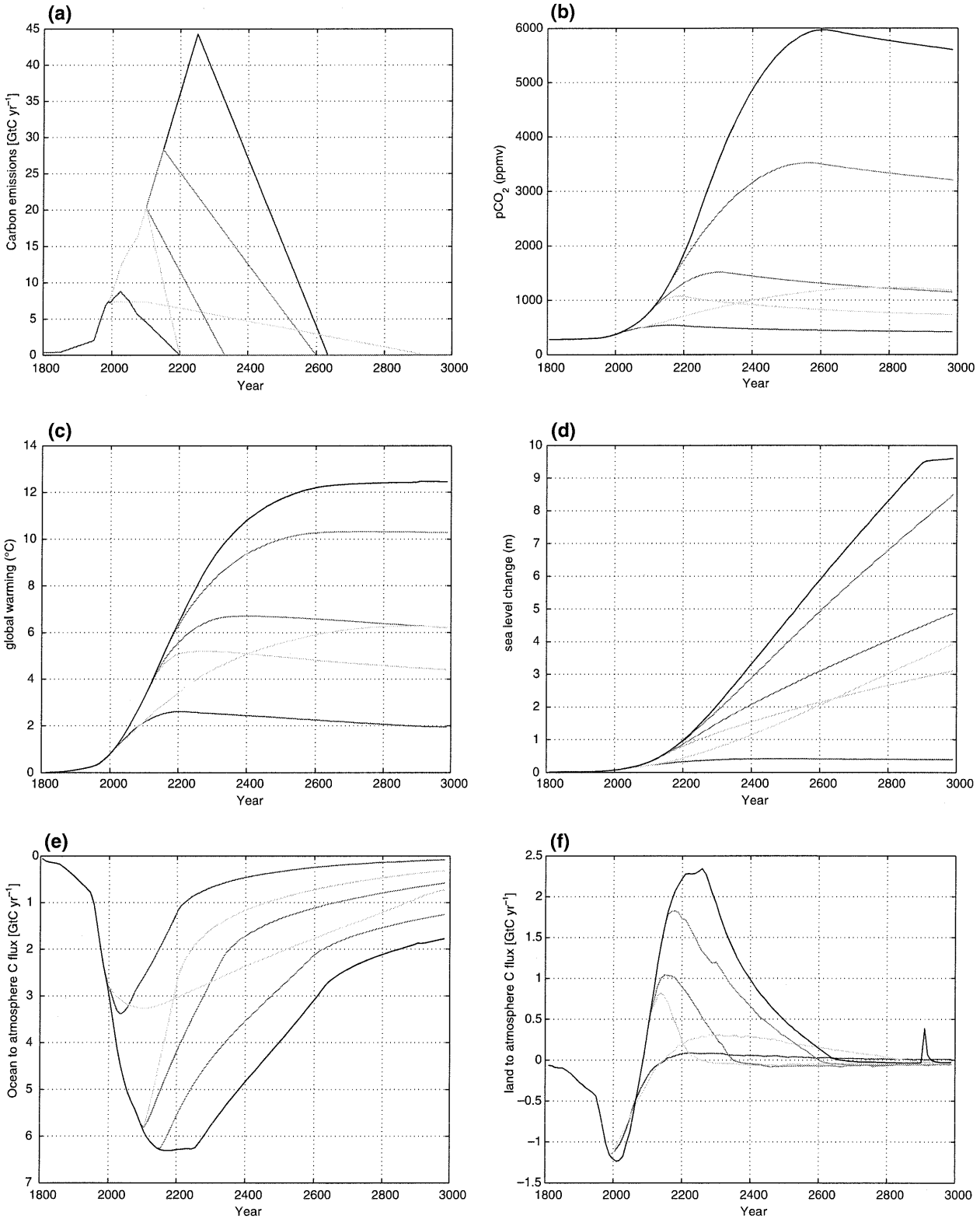

Fig. 9 Long-term **a** CO_2 emissions, and for the traceable climate parameter set, projections of; **b** atmospheric CO_2, **c** global annual mean surface air temperature change, **d** sea level rise, **e** ocean-atmosphere CO_2 exchange, **f** land-atmosphere CO_2 exchange. Emissions scenarios (Table 2) have corresponding colours: *A* navy, *B* green, *C* red, *D* cyan, *E* magenta, *F* black

Table 5 The fraction of added CO_2 remaining in the atmosphere at the end of the millennium (airborne fraction) for each scenario and model variant

Scenario	Model variant		
	Subjective	Traceable	Objective
A	0.23	0.27	0.26
B	0.28	0.37	0.31
C	0.35	0.47	0.38
D	0.37	0.49	0.39
E	0.66	0.79	0.67
F	0.67	0.76	0.67

versions. The subjectively tuned parameter set has approximately twice the range of warming of the other two, primarily due to its weaker atmospheric heat diffusion combined with the loss of Antarctic sea ice. The impact of weakening or collapse of the ocean thermohaline circulation is revealed in an amplified warming in the Southern Ocean and the weakest warming being in the North Atlantic. This is clearest for the traceable version.

The spatial patterns of precipitation change (Fig. 10) show a consistent drying across desert regions of the world and a wetting everywhere else that is greatest over boreal forest and where sea-ice is lost from the Southern Ocean. The overall magnitude and range of precipitation change is generally smallest in the objectively tuned and greatest in the traceable version. However, the Amazon and Indonesian rainforests stand out as getting significantly wetter in the subjectively tuned version, slightly wetter in the objectively tuned version, but not changing in the traceable version.

5.3 Carbon cycle

The long-term response of the present ocean and land carbon sinks is shown in Fig. 9e, f. The ocean is a robust carbon sink. It continues to grow until emissions decline and the growth rate of CO_2 in the atmosphere begins to slow, after which the gradient of CO_2 between the atmosphere and ocean that drives the sink begins to decline. Notably, in the 15,000 GtC scenario F, the ocean carbon sink does not get significantly larger than in the ≈9,200 GtC scenario E, despite emissions continuing to increase. This is presumably due to an almost complete loss of buffering capacity of the carbonate system in the ocean.

The land carbon sink is not robust and the land surface can become a significant carbon source in the future. The sink-source switch occurs around 2090 following business as usual in four out of six scenarios, and is due to warming induced increases in CO_2 loss from plant and soil respiration exceeding CO_2 fertilization induced increases in CO_2 uptake by photosynthesis. The land carbon sink disappears around 2150 in the other two scenarios (which have much lower emissions at this time) due to respiratory CO_2 losses coming back into balance with photosynthetic CO_2 uptake. The land carbon source only achieves significant magnitude if emissions continue to increase as in scenarios B, C, E and F, it cancels the earlier land carbon sink in scenario C and is much larger for scenarios E and F. In the 15,000 GtC scenario F a small transient loss of land carbon occurs just after 2900, which is associated with the end of Greenland melt and a corresponding change in ocean circulation and heat transport. A slight warming on either side of the North Atlantic leads to a loss of carbon from Western Europe and Eastern Canada. No such land carbon source is generated in the subjectively tuned parameter version when Greenland finishes melting.

Changes in carbon storage in vegetation and soil in year 3000 relative to the initial state are shown in Fig. 11 for scenarios A, C and F in the traceable version. In the minimum emissions scenario A, vegetation carbon increases in most regions, due to CO_2 fertilization of photosynthesis dominating, and soil carbon increases in the boreal regions. In the 4,000 GtC fast scenario C, vegetation carbon increases in most regions except central Africa and parts of China, boreal soil carbon tends to increase but soil carbon is lost from other regions. The loss of soil carbon is due to soil respiration being increased by warming in excess of the increase in litter fall from more productive vegetation. In the 15,000 GtC scenario F, vegetation loses carbon in central Africa, Amazonia, SE Asia and NW Australasia (the warmest regions in the model) whilst gaining carbon elsewhere. Soil carbon is lost almost everywhere except in N Canada and central Asia. The dieback of tropical vegetation is due to excessive warmth, bearing in mind that the model tropics are too cold in the present state.

These results are robust across the model variants except for the response of Amazonia, which experiences either a modest (objective) or significant (subjective) increase in precipitation and consequently gains vegetation carbon even under the extreme 15,000 GtC forcing. In the objective model, Amazonia still loses soil carbon due to warming, but in the subjective model the increase in precipitation is sufficient to allow Amazonia to gain soil carbon.

Average ocean surface pH drops from an initial value of 8.15 as added CO_2 enters the ocean. The change depends inversely on atmospheric CO_2 with maximum changes in pH units being: (A) −0.2, (B) −0.4, (C) −0.55, (D) −0.45, (E) −0.9, (F) −1.15. The primary control is total carbon emitted but the rate of emissions also has an effect on transient pH minima.

5.4 Ocean circulation

The response of the Atlantic Meridional Overturning Circulation (MOC) is highly sensitive to uncertain model climate parameters and somewhat sensitive to the inclusion of Greenland ice sheet melt (Fig. 12).

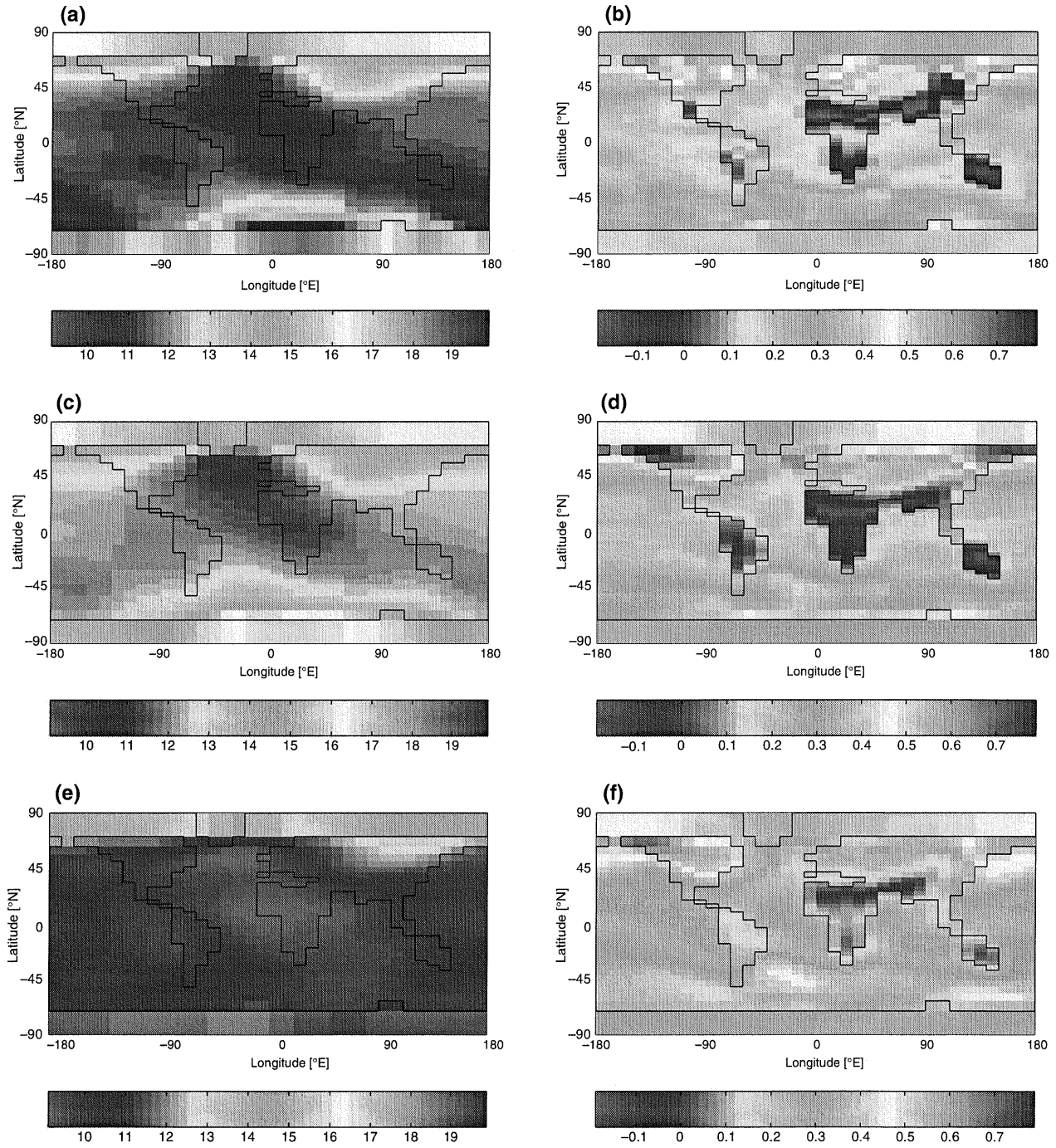

Fig. 10 Patterns of temperature and precipitation change from the pre-industrial state to year 3000 under 15,000 GtC emissions scenario F: **a**, **c**, **e** air temperature change (°C) **b**, **d**, **f** precipitation change (m year^{-1}), for model climate parameter sets **a**–**b** subjective **c**–**d** traceable **e**–**f** objective

Both traceable and objective parameter sets are prone to MOC collapse, with the traceable set being most sensitive. The subjectively tuned parameter set is not prone to MOC collapse, recalling that it starts with the strongest MOC.

In all model variants and emissions scenarios, increasing forcing weakens the strength of the Atlantic MOC. Weakening of the MOC persists to the end of the millennium, and the degree of weakening depends on the total carbon emitted and is insensitive to the rate of

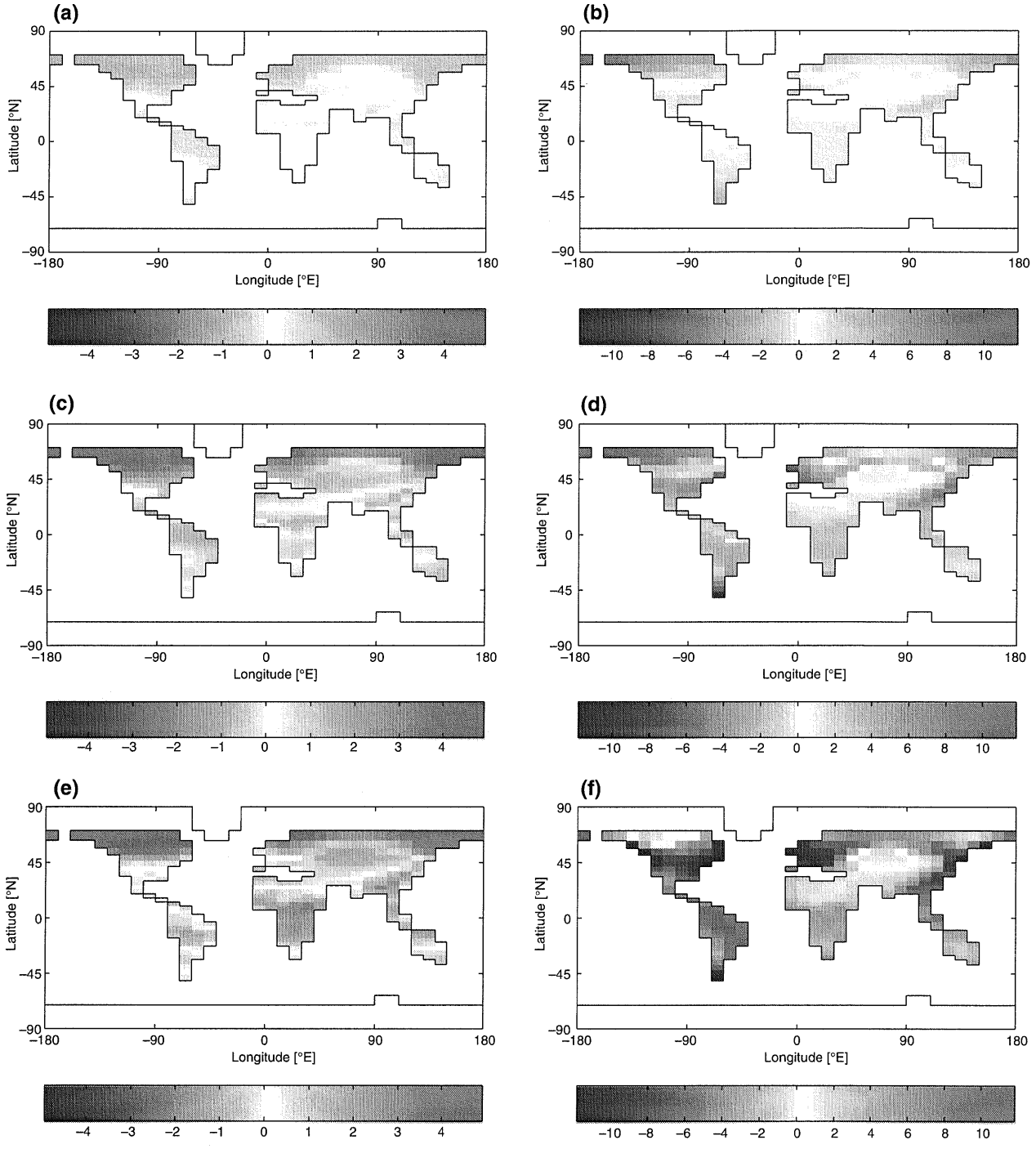

Fig. 11 Change in carbon storage (kgC m^{-2}) in vegetation (**a**, **c**, **e**) and soil (**b**, **d**, **f**) in year 3000 relative to 1800 for the traceable climate parameter set and emissions scenarios **a**, **b** A 1,100 GtC, **c**, **d** C 4,000 GtC fast, and **e**, **f** F 15,000 GtC

emissions once they are complete, contradicting the results of Stocker and Schmittner (1997). It takes extreme emissions of 9,200 or 15,000 GtC and the freshwater flux from Greenland ice sheet melt to trigger MOC collapse in the objective parameter version, but in the traceable version under 15,000 GtC emissions, sustained MOC collapse occurs without a Greenland meltwater flux. In the subjectively tuned model version, when Greenland finishes melting under 15,000 GtC emissions, the Atlantic MOC strengthens markedly within decades due to the resumption of deep water formation. However, in the traceable model version,

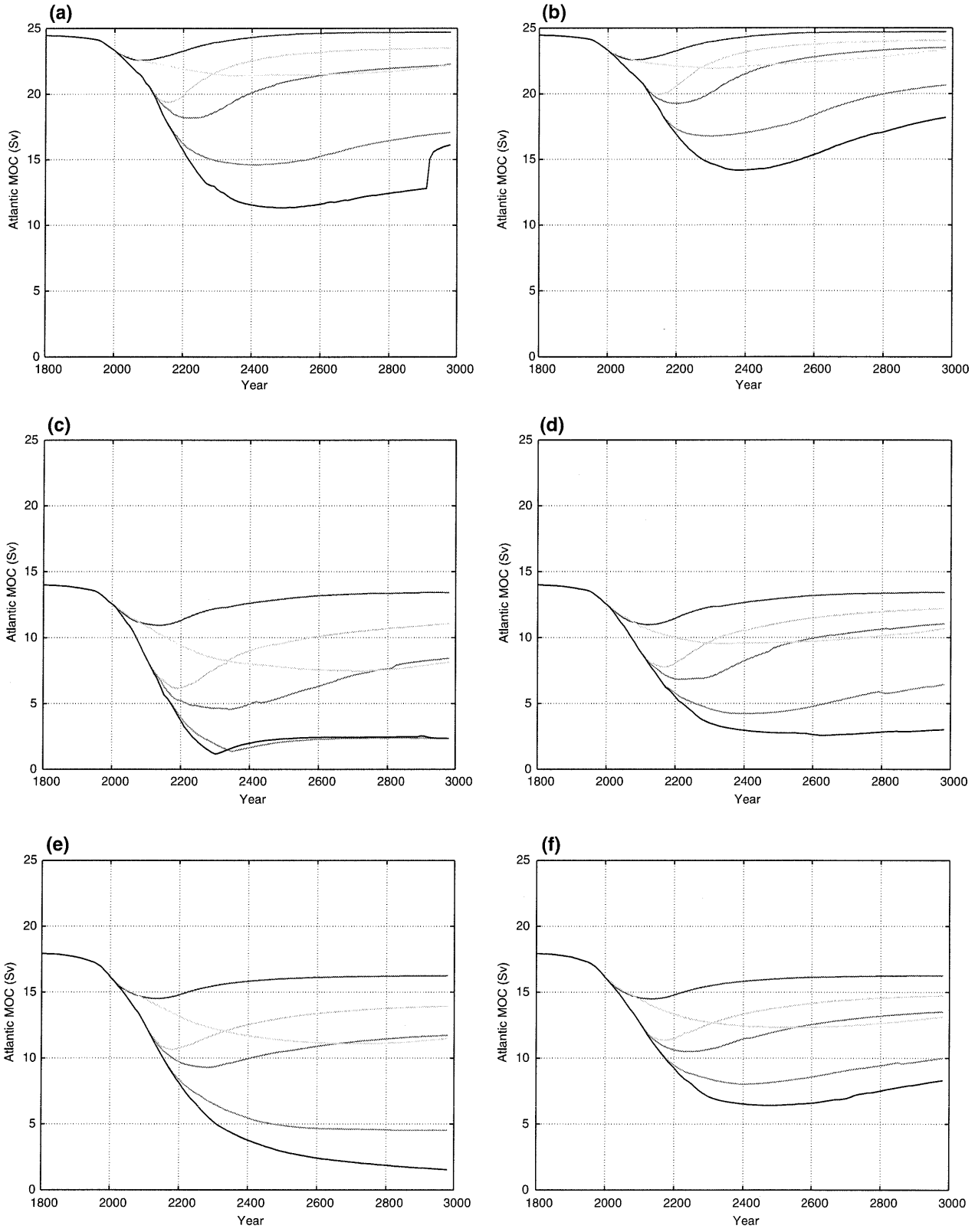

Fig. 12 Response of the Atlantic Meridional Overturning Circulation (MOC) (**a**, **c**, **e**) with, or (**b**, **d**, **f**) without, Greenland ice sheet melt water being added to the cells surrounding Greenland, for different model climate parameter sets; **a**–**b** subjective, **c**–**d** traceable, **e**–**f** objective. Emissions scenarios (Table 2) have corresponding colours: *A* navy, *B* green, *C* red, *D* cyan, *E* magenta, *F* black

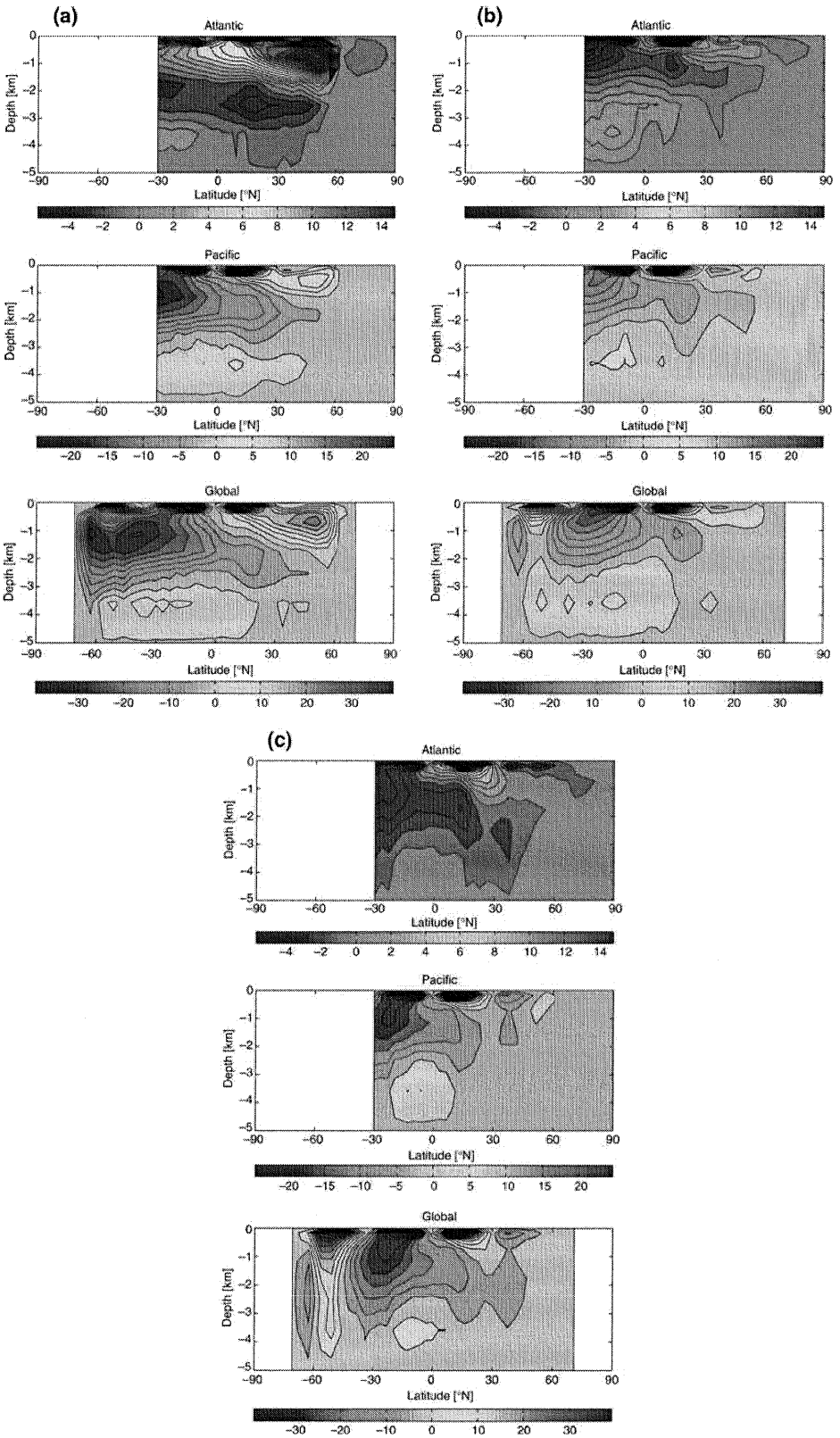

Fig. 13 Atlantic, Pacific and Global Meridional Overturning Circulation (MOC), in year 3000 of the 15,000 GtC scenario, for different model climate parameter sets; **a** subjective, **b** traceable, **c** objective

when Greenland finishes melting, only a slight blip in Atlantic MOC strength is apparent, yet resultant changes in ocean heat transport trigger a transient land carbon source (described above).

Contrasting the meridional overturning circulation in year 3000 after 15,000 GtC emissions and including the contribution of Greenland melt (Fig. 13) with the pre-industrial state (Fig. 4) shows some interesting features. The response of the subjectively tuned model is typical of MOC weakening without collapse across the model variants and scenarios. Both positive Atlantic MOC and negative Pacific MOC cells get shallower. What was Antarctic Bottom Water (AABW) in the Atlantic shifts upward to intermediate depths. Thus the deep Atlantic below about 4km and the deep Pacific below about 3km become more isolated from exchange with the surface ocean and atmosphere. The response of the traceable and objective parameter versions are similar and illustrative of MOC collapse. The Atlantic has a reversed circulation that is weaker than the corresponding Pacific circulation. The depth of the main meridional overturning cells is noticeably greater in the objective version than the traceable version.

6 Discussion

The GENIE-1 results highlight that total CO_2 emitted exerts the dominant control on climate change on the millennial timescale, with rate of emissions having a secondary effect, especially on sea level. Given a mid-range climate sensitivity, emitting conventional fossil fuel resources of 4,000 GtC leads to over 1,000 ppmv CO_2 and 6°C global warming on the millennial timescale, regardless of the rate of emissions. Sea level rise in year 3000 is 4–5 m, depending on the rate of emissions, and ongoing. Emitting exotic fossil fuel resources to give total emissions of up to 15,000 GtC leads to unthinkable climate changes of over 12°C global warming and up to 10 m sea level rise on the millennial timescale.

The atmospheric CO_2 projections of GENIE-1 can be directly compared with those from a simple box model (Lenton 2000) forced with the same emissions scenarios (Lenton 2006). Peak CO_2 is typically 10% higher for a given emissions scenario in the traceable version of GENIE-1. This is primarily because it has a weaker future ocean carbon sink than the box model (although it also has a smaller land carbon source). Global warming is greater in GENIE-1 for 4,000 GtC emissions or less because the box model has lower CO_2 and a slightly lower climate sensitivity of 2.8°C. However, global warming is much less in GENIE-1 for 9,200 GtC or 15,000 GtC emissions, because the box model has a significant increase in climate sensitivity for each subsequent doubling of CO_2.

The switch from a land carbon sink to a source in GENIE-1 is qualitatively similar to that seen in the Hadley Centre C4GCM, HadCM3LC (Cox et al. 2000; Jones et al. 2003), but in the IPSL C4GCM the land carbon sink grows and then stabilizes (Berthelot et al. 2002). In both HadCM3LC and GENIE-1, the land carbon source is dominated by loss of global soil carbon. The sink-source transition occurs later in GENIE-1 than HadCM3LC—2090 as opposed to 2030 (Cox et al. 2000) or 2040 (Jones et al. 2003)—and the source generated is of smaller magnitude. This can be attributed to a slower rate of global warming in GENIE-1 (3.5°C as opposed to 5°C in 2100) and in particular less land surface warming (in HadCM3LC the land surface warms 8°C in 2100). Furthermore, the temperature sensitivity of soil respiration declines with increasing temperature in GENIE-1 (consistent with field data), whilst HadCM3LC assumes that the sensitivity is constant (a doubling of rate for every 10°C warming). A sink-source transition can also be forced on the century timescale in other coupled models (Joos et al. 2001; Matthews et al. 2005; Thompson et al. 2004; Zeng et al. 2004), but a persistent land carbon sink is seen in some (Fung et al. 2005; Matthews et al. 2005; Thompson et al. 2004). Furthermore, when six Dynamic Global Vegetation Models are driven off-line with a business as usual (IS92a) CO_2 concentration scenario and corresponding climate change, only one becomes a land carbon source around 2100, in the other five the land remains a carbon sink (Cramer et al. 2001). Whether a sink-source transition occurs can be sensitive to the assumed response of photosynthesis to CO_2 fertilization (Thompson et al. 2004) or temperature (Matthews et al. 2005). In GENIE-1 net primary productivity robustly increases on the century timescale, however future sensitivity studies should vary these responses.

The robust growth of the ocean carbon sink in GENIE-1 is consistent with other models (Joos et al. 1999; Sarmiento et al. 1998), as is its size under business as usual forcing, of nearly 6 GtC $year^{-1}$ in 2100. The apparent capping of the ocean carbon sink in GENIE-1 under extreme 15,000 GtC forcing, despite increasing emissions, is an interesting result that deserves further investigation. The predicted ocean surface pH changes are consistent with those found by Caldeira and Wickett (2003) and could exceed those seen in the past 300 million years. They may have the potential to severely disrupt marine calcifying organisms including calcareous plankton and corals.

The GENIE-1 prediction that the world can continue to warm when CO_2 is stabilized is consistent with GCM studies, as is the amplified warming of the high latitudes and the greater rate of warming over land than ocean, although the ratio of land to ocean warming varies considerably between GCMs. Our results show that by the end of the millennium, land and sea at a given latitude may have warmed a similar amount because they are approaching equilibrium, thus removing the impact of heat capacity, which slows the transient warming of the ocean. The predicted decline in Northern Hemisphere sea-ice extent is consistent with observations and the future projections are conservative when compared to GCM predictions for the twenty-first century

(Houghton et al. 2001). However, GENIE-1 underestimates current Southern Hemisphere sea-ice extent and predicts a greater sensitivity of Southern Hemisphere than Northern Hemisphere sea-ice cover, whilst GCMs suggest the converse (Houghton et al. 2001).

The sea level rise due to thermal expansion in GENIE-1 is at the lower end of the range from existing models which on a millennial timescale predict 0.5–2 m for doubling CO_2 and 1–4 m for quadrupling CO_2 (Houghton et al. 2001). The Greenland melt parameterization is prescribed from a single existing study, which has been used elsewhere (Gregory et al. 2004). The model-derived threshold of 2.6°C for triggering net mass loss (Huybrechts and Wolde 1999) may be too high given recent inferences that Greenland is already contributing to sea level rise (Rignot and Thomas 2002; Mitrovica et al. 2001) although the overall mass balance of the Greenland ice sheet remains uncertain (Johannessen et al. 2005). The modelled timescale of $\approx 10^3$ year for ice sheet collapse may also be conservative, given rates of sea level rise at the last deglaciation and mechanisms that are missing from existing ice-sheet models (Hansen 2005). The contribution of Antarctica and of other inland ice is ignored in our simulations. Extra snow accumulation on the East Antarctic ice sheet could lower sea level by 0.6 m on the millennial timescale but potential mass loss from the West Antarctic Ice Sheet could raise it by 0.8 m (Huybrechts and Wolde 1999). Hence our sea-level projections should be treated as minimum estimates, for a given emissions scenario.

The impact of Greenland meltwater weakening the Atlantic Meridional Overturning Circulation (MOC) and potentially contributing to its collapse has also been seen in a coupled AOGCM-ice sheet model on the century timescale (Fichefet et al. 2003). This represents a negative feedback on Greenland ice sheet melt in that it reduces the ocean heat transport to the North Atlantic and will thus slow the rate of warming there, and may even temporarily cause a cooling over SE Greenland (Fichefet et al. 2003). The negative feedback is very weak in GENIE-1, for example in the 15,000 GtC scenario if we do not allow the addition of Greenland meltwater to the ocean we find that the melt of Greenland completes only a few decades earlier.

The response of the Atlantic MOC in GENIE-1 and C-GOLDSTEIN is the most sensitive aspect of the models to uncertain parameters. Earlier work with C-GOLDSTEIN (Annan et al. 2005; Hargreaves et al. 2004) has shown that uncertainty in the initial conditions (i.e. the current strength of the MOC) combined with model uncertainty and the potential for the MOC to be close to a non-linear threshold mean that its behaviour may be fundamentally unpredictable (Knutti and Stocker 2002). In this study we find two out of three model variants prone to MOC collapse but it requires extreme forcing, i.e. burning of exotic fossil fuels. The magnitude of MOC weakening for a given emissions scenario is similar across the three model variants and the contribution of Greenland ice sheet melt is smaller than that of global warming. This can be understood in terms of the sensitivity of the freshwater balance of the North Atlantic to warming.

Rahmstorf and Ganopolski (1999) define a hydrological sensitivity parameter that linearly relates the extra freshwater flux to the N. Atlantic to the increase in Northern Hemispheric temperature. Ignoring Greenland melt and considering the balance of runoff plus precipitation minus evaporation, the increase in freshwater flux to the Atlantic Ocean above 50 N and the Arctic Ocean, under CO_2 doubling, is 0.10 Sv (subjective), 0.11 Sv (traceable), 0.12 Sv (objective) giving sensitivities per degree of global warming of 0.030 Sv/°C, 0.034 Sv/°C and 0.043 Sv/°C. These are comparable to the 0.03 Sv/°C in the GCM of Manabe and Stouffer (1994). Our parameterization of Greenland melt implies a linear relationship between warming over Greenland (above a threshold of 2.6°C above pre-industrial) and freshwater flux to the ocean grid cells around Greenland of 0.011 Sv/°C. Hence the total sensitivity of GENIE-1 is in the range of values of 0.03–0.05 Sv/°C experimented with in CLIMBER-2, yet it proves much harder to trigger MOC collapse in GENIE-1.

Weakening of the MOC in GENIE-1 persists to the end of the millennium, and the degree of weakening depends on the total carbon emitted. Furthermore, once emissions are complete, the resulting change in MOC strength is insensitive to the rate at which a given amount of fossil fuel was emitted. This contradicts the results of Stocker and Schmittner (1997) using the Bern 2.5D model, but agrees with results from the CLIMBER-2 model (A. Ganopolski, personal communication). Given that these two other coupled models use the same ocean component, sensitivity or insensitivity of the MOC strength to rate of forcing appears to be determined by the choice of atmosphere model.

7 Conclusion

We have described a new Earth system model, GENIE-1, and its application to examining carbon cycle and climate change on a millennial timescale. The strength of the model is its computational efficiency, which allows us to undertake extensive model tuning, long integrations, and large ensemble sensitivity studies, capabilities which we have only begun to exploit in the present work. Here we have explored the millennial timescale impact of the conceivable range of total fossil fuel CO_2 emissions and the effect of rate of emissions. Atmospheric CO_2 will have approached equilibrium in year 3000 and even for our minimum emissions scenario (1,100 GtC) will be 1.5 times the pre-industrial level at 420 ppmv, giving 1.5°C global warming. For our most extreme emissions scenario (15,000 GtC), CO_2 peaks at 6,000 ppmv giving 12.5°C global warming. Minimizing emissions will largely avoid an assumed Greenland ice sheet melt threshold of 2.6°C local warming, allowing sea level rise to stabilize at 0.4 m and Atlantic meridional overturning

circulation to recover from a temporary weakening, minimizing surface ocean acidification to a drop of 0.2 pH units, and avoiding a transient land carbon source. In contrast, maximizing emissions causes complete Greenland melt by year 3000, 10 m of ongoing sea level rise, possible collapse of the Atlantic meridional overturning circulation, a 1.15 unit drop in ocean surface pH, huge loss of global soil carbon and dieback of some tropical and sub-tropical vegetation. Future work will add a carbonate sediment module to GENIE-1 and consider how long it takes to recover pre-industrial CO_2 and climate from different sizes of fossil fuel perturbation.

Acknowledgements This work is a joint output of the Grid ENabled Integrated Earth system model (GENIE) project of the UK Natural Environment Research Council (NERC) e-Science programme (NER/T/S/2002/00217) and the Tyndall Centre for Climate Change Research (T3.18).

References

Adams B, White A, Lenton TM (2004) An analysis of some diverse approaches to modelling net primary productivity. Ecol Modell 177:353–391

Annan JD, Hargreaves JC, Edwards NR, Marsh R (2005) Parameter estimation in an intermediate complexity earth system model using an ensemble Kalman filter. Ocean Modell 8:135–154

Archer D, Kheshgi H, Maier-Reimer E (1998) Dynamics of fossil fuel CO_2 neutralization by marine $CaCO_3$. Global Biogeochem Cycles 12:259–276

Batjes NH (1995) A homogenized soil data file for global environmental research: a subset of FAO, ISRIC and NRCS profiles (version 1.0). Working Paper and Preprint 95/10b, International Soil Reference and Information Centre, Wageningen, The Netherlands

Beltran C, Edwards NR, Haurie A, Vial J-P, Zachary DS (2005) Oracle-based optimisation applied to climate model calibration. Environ Modell Assess, DOI: 10.1007/s10666-005-9024-4

Berthelot M, Friedlingstein P, Ciais P, Monfray P, Dufrense JL, Treut HL, Fairhead L (2002) Global response of the terrestrial biosphere to CO_2 and climate change using a coupled climate–carbon cycle model. Global Biogeochem Cycles 16:1084

Briegleb BP, Minnis P, Ramanathan V, Harrison E (1986) Comparison of regional clear-sky albedos inferred from satellite observations and model comparisons. J Climatol Appl Meterol 25:214–226

Caldeira K, Wickett ME (2003) Anthropogenic carbon and ocean pH. Nature 425:365

Cameron DR, Lenton TM, Ridgwell AJ, Shepherd JG, Marsh R (2005) A factorial analysis of the marine carbon cycle and ocean circulation controls on atmospheric CO_2. Global Biogeochem Cycles 19:GB4027

Claussen M, Mysak L, Weaver A, Crucifix M, Fichefet T, Loutre M, Weber S, Alcamo J, Alexeev V, Berger A, Calov R, Ganopolski A, Goosse H, Lohmann G, Lunkeit F, Mokhov I, Petoukhov V, Stone P, Wang Z (2002) Earth system models of intermediate complexity: closing the gap in the spectrum of climate system models. Clim Dyn 18:579–586

Cox PM, Betts RA, Jones CD, Spall SA, Totterdell IJ (2000) Acceleration of global warming due to carbon-cycle feedbacks in a coupled climate model. Nature 408(6813):184–187

Cramer W, Bondeau A, Woodward FI, Prentice IC, Betts RA, Brovkin V, Cox PM, Fisher V, Foley JA, Friend AD, Kucharik C, Lomas MR, Ramankutty N, Sitch S, Smith B, White A, Young-Molling C (2001) Global response of terrestrial ecosystem structure and function to CO_2 and climate change: results from six dynamic global vegetation models. Glob Change Biol 7:357–373

Edwards NR, Marsh R (2005) Uncertainities due to transport-parameter sensitivity in an efficient 3-D ocean-climate model. Clim Dyn 24:415–433

Essery R, Best M, Cox P (2001) MOSES 2.2 technical documentation. Tech Rep 30, Hadley Centre

Fanning AG, Weaver AJ (1996) An atmospheric energy-moisture model: climatology, interpentadal climate change and coupling to an ocean general circulation model. J Geophys Res 101:15111–15128

Fichefet T, Poncin C, Goosse H, Huybrechts P, Janssens I, Le Treut H (2003) Implications of changes in freshwater flux from the Greenland ice sheet for the climate of the 21st century. Geophys Res Lett 30:1911

Friedlingstein P, Bopp L, Ciais P, Dufresne J-L, Fairhead L, LeTreut H, Monfray P, Orr J (2001) Positive feedback between future climate change and the carbon cycle. Geophys Res Lett 28(8):1543–1546

Friedlingstein P, Cox P, Betts R, Bopp L, Bloh Wv, Brovkin V, Doney S, Eby M, Fung I, Govindasamy B, John J, Jones C, Joos F, Kato T, Kawamiya M, Knorr W, Lindsay K, Matthews HD, Raddatz T, Rayner P, Reick C, Roeckner E, Schnitzler K-G, Schnur R, Strassmann K, Thompson S, Weaver A, Yoshikawa C, Zeng N (2006) Climate-carbon cycle feedback analysis, results from the C4MIP model intercomparison. J Clim (in press)

Fung IY, Doney SC, Lindsay K, John J (2005) Evolution of carbon sinks in a changing climate. Proc Nat Acad Sci 32(102):11201–11206

Ganachaud A, Wunsch C (2000) Improved estimates of global ocean circulation, heat transport and mixing from hydrographic data. Nature 408:453–457

Gregory JM, Huybrechts P, Raper SCB (2004) Threatened loss of the Greenland ice-sheet. Nature 428:616

Hansen JE (2005) A slippery slope: how much global warming constitutes "dangerous anthropogenic interference"? Clim Change 68:269–279

Hargreaves JC, Annan JD, Edwards NR, Marsh R (2004) An efficient climate forecasting method using an intermediate complexity Earth System Model and the ensemble Kalman filter. Clim Dyn 23:745–760

Hasselmann K, Hasselmann S, Giering R, Ocana V, Storch H (1997) Sensitivity study of optimal CO_2 emissions path using a simplified structural integrated assessment model (SIAM). Clim Change 37:345–386

Hasselmann K, Latif M, Hooss G, Azar C, Edenhofer O, Jaeger CC, Johannessen OM, Kemfert C, Welp M, Wokaun A (2003) The challenge of long-term climate change. Science 302:1923–1925

Hibler WD (1979) A dynamic thermodynamic sea ice model. J Phys Oceanogr 9:815–846

Houghton RA, Hackler JL (2002) Carbon flux to the atmosphere from land-use changes. Trends: a compendium of data on global change. Tech. rep., Carbon Dioxide Information Analysis Center, Oak Ridge National Laboratory, Oak Ridge, Tenn., USA

Houghton JT, Jenkins GJ, Ephraums JJ (1990) Climate change. The IPCC scientific assessment. Cambridge University Press, Cambridge

Houghton JT, Filho LGM, Callander BA, Harris N, Kattenberg A, Maskell K (1995) Climate change 1995. The science of climate change. Cambridge University Press, Cambridge

Houghton JT, Ding Y, Griggs DJ, Noguer M, van der Linden PJ, Dai X, Maskell K, Johnson CA (eds) (2001) Climate change 2001: the scientific basis. Cambridge University Press, Cambridge

House JI, Prentice IC, Ramankutty N, Houghton R, Heimann M (2003) Reconciling apparent inconsistencies in estimates of terrestrial CO_2 sources and sinks. Tellus B 53B:345–363

Huybrechts P, Wolde JD (1999) The dynamic response of the Greenland and Antarctic ice sheets to multiple-century climatic warming. J Clim 12:2169–2188
Johannessen OM, Khvorostovsky K, Miles MW, Bobylev LP (2005) Recent ice-sheet growth in the interior of Greenland. Science 310:1013–1016
Jones DR, Schonlau M, Welch WJ (1998) Efficient global optimization of expensive black-box functions. J Glob Optim 13(4):455–492
Jones CD, Cox PM, Essery RLH, Roberts DL, Woodgate MJ (2003) Strong carbon cycle feedbacks in a climate model with interactive CO_2 and sulphate aerosols. Geophys Res Lett 30:1479
Joos F, Plattner G-K, Stocker T, Marchal O, Schmittner A (1999) Global warming and marine carbon cycle feedbacks on future atmospheric CO_2. Science 284:464–467
Joos F, Prentice IC, Sitch S, Meyer R, Hooss G, Plattner G-K, Gerber S, Hasselmann K (2001) Global warming feedbacks on terrestrial carbon uptake under the Intergovernmental Panel on Climate Change (IPCC) emission scenarios. Global Biogeochem Cycles 15:891–907
Keane AJ (2003) Wing optimization using design of experiment, response surface and data fusion methods. J Aircr 40(4):741–750
Keeling C, Whorf TP (2005) Atmospheric CO_2 records from sites in the SIO air sampling network. Tech. rep., Carbon Dioxide Information Analysis Center, Oak Ridge National Laboratory, U.S. Department of Energy, Oak Ridge, Tenn., USA
Killworth PD (1996) Time interpolation of forcing fields in ocean models. J Phys Oceanogr 26:126–143
Kirschbaum MU (1995) The temperature dependence of soil organic matter decomposition, and the effect of global warming on soil organic storage. Soil Biol Biochem 27(6):753–760
Knutti R, Stocker TF (2002) Limited predictability of the future thermohaline circulation close to an instability threshold. J Clim 15:179–186
Lenton TM (2000) Land and ocean carbon cycle feedback effects on global warming in a simple Earth system model. Tellus 52B:1159–1188
Lenton TM (2006) Climate change to the end of the millennium. Clim Change (in press)
Lenton TM, Cannell MGR (2002) Mitigating the rate and extent of global warming. Clim Change 52:255–262
Lenton TM, Huntingford C (2003) Global terrestrial carbon storage and uncertainties in its temperature sensitivity examined with a simple model. Glob Change Biol 9:1333–1352
Lloyd J, Taylor JA (1994) On the temperature-dependence of soil respiration. Funct Ecol 8(3):315–323
Manabe S, Stouffer RJ (1994) Multiple-century response of a coupled ocean–atmosphere model to an increase of atmospheric carbon dioxide. J Clim 7:5–23
Marland G, Boden TA, Andres RJ (2003) Global, regional, and national fossil fuel CO_2 emissions. Trends: a compendium of data on global change. Tech. rep., Carbon Dioxide Information Analysis Center, Oak Ridge National Laboratory, Oak Ridge, Tenn., USA
Matthews E (1985) Atlas of archived vegetation, land use, and seasonal albedo data sets. NASA Technical Memorandum 86199, Goddard Institute for Space Studies, New York
Matthews HD, Eby M, Weaver AJ, Hawkins BJ (2005) Primary productivity control of simulated carbon cycle-climate feedbacks. Geophys Res Lett 32:L14708
Meehl GA, Washington WM, Collins WD, Alblaster JM, Hu A, Buja LE, Strand WG, Teng H (2005) How much more global warming and sea level rise? Science 307:1769–1772
Miller L, Douglas BC (2004) Mass and volume contributions to twentieth-century global sea level rise. Nature 428:406–409
Mitrovica JX, Tamislea ME, Davis JL, Milne GA (2001) Recent mass balance of polar ice sheets inferred from patterns of sea-level change. Nature 409:1026–1029
Myers RH, Montgomery DC (1995) Response surface methodology: process and product optimization using design of experiments. Wiley, New York
Olson JS, Watts JA, Allison LJ (1985) Major world ecosystem complexes ranked by carbon in live vegetation. Tech. Rep. NDP-017, Carbon Dioxide Information Analysis Center, Oak Ridge National Laboratory, Oak Ridge, Tennessee
Parkinson C (2002) Trends in the length of the southern ocean sea-ice season, 1979–99. Ann Glaciol 34(1):435–440
Parkinson C, Cavalieri D, Gloersen P, Zwally H, Comiso J (1999) Arctic sea ice extents, areas and trends, 1978–1996. J Geophys Res (Oceans) 104(C9):20837–20856
Peixoto JP, Oort AH (1991) Physics of climate. 520pp. AIP Press
Plattner G-K, Joos F, Stocker TF, Marchal O (2001) Feedback mechanisms and sensitivities of ocean carbon uptake under global warming. Tellus 53B:564–592
Price AR, Xue G, Yool A, Lunt DJ, Valdes PJ, Lenton TM, Wason JL, Pound GE, Cox SJ, the GENIE team (2006) Optimisation of integrated earth system model components using grid-enabled data management and computation. Concurrency and Computation: Practice and Experience (in press)
Rahmstorf S, Ganopolski A (1999) Long term global warming scenarios computed with an efficient coupled climate model. Clim Change 43:353–367
Ridgwell AJ (2001) Glacial-interglacial perturbations in the global carbon cycle. Ph.D. thesis, University of East Anglia
Rignot E, Thomas RH (2002) Mass balance of polar ice sheets. Science 297:1502–1506
Sabine CL, Feely RA, Gruber N, Key RM, Lee K, Bullister JL, Wanninkhof R, Wong CS, Wallace DWR, Tilbrook B, Millero FJ, Peng T-H, Kozyr A, Ono T, Rios AF (2004) The oceanic sink for anthropogenic CO_2. Science 305:367–371
Sarmiento JL, Hughes TMC, Stouffer RJ, Manabe S (1998) Simulated response of the ocean carbon cycle to anthropogenic climate warming. Nature 393:245–249
Semtner AJ (1976) A model for the thermodynamic growth of sea ice in numerical investigations of climate. J Phys Oceanogr 6:379–389
Statnikov RB, Matuzov JB (1995) Multicriteria optimization and engineering. Chapman and Hall, New York
Stocker TF, Schmittner A (1997) Influence of CO_2 emission rates on the stability of the thermohaline circulation. Nature 388:862–865
Stroeve JC, Serreze MC, Fetterer F, Arbetter T, Meier W, Maslanik J, Knowles K (2005) Tracking the Arctic's shrinking ice cover: another extreme September minimum in 2004. Geophys Res Lett 32:L04501
Takahashi T, Sutherland SC, Sweeney C, Poisson A, Metzl N, Tillbrook B, Bates N, Wanninkhof R, Feely RA, Sabine C, Olafsson J, Nojiri Y (2002) Global sea-air CO_2 flux based on climatological surface ocean pCO_2, and seasonal biological and temperature effects. Deep-Sea Res II 49:1601–1622
Thompson SL, Govindasamy B, Mirin A, Caldeira K, Delire C, Milovich J, Wickett M, Erickson D (2004) Quantifying the effects of CO_2-fertilized vegetation on future global climate and carbon dynamics. Geophys Res Lett 31:L23211
Toggweiler JR, Samuels B (1998) On the ocean's large-scale circulation near the limit of no vertical mixing. J Phys Oceanogr 28(9):1832–1852
Weaver AJ, Eby M, Weibe EC, Bitz CM, Duffy PB, Ewen TL, Fanning AF, Holland MM, MacFadyen A, Matthews HD, Meissner KJ, Saenko O, Schmittner A, Wang H, Yoshimori M (2001) The UVic earth system climate model: Model description, climatology, and applications to past, present and future climates. Atmos-Ocean 39(4):361–428
Williamson MS, Lenton TM, Shepherd JG, Edwards NR (2006) An efficient numerical terrestrial scheme (ENTS) for fast earth system modelling. Tyndall Centre Working Paper 83
Yuret D, Maza M (1993) Dynamic hill climbing: overcoming the limitations of optimization techniques. In: Proceedings of the second Turkish symposium on artificial intelligence and neural networks, pp 254–260
Zeng N, Qian H, Munoz E, Iacono R (2004) How strong is carbon cycle-climate feedback under global warming. Geophys Res Lett 31:L20203